OPTICAL PHOTON-ACOUSTIC PHONON INTERACTIONS; STIMULATED BRILLOUIN SCATTERING

by

A. Pine

ERL Technical Memorandum M-117

22 November 1965

ELECTRONICS RESEARCH LABORATORY

College of Engineering
University of California, Berkeley
94720

The research herein was supported in part by the Joint Services Electronics Program (Air Force Office of Scientific Research, Army Research Office, Office of Naval Research) under Grant AF-AFOSR-139-65 and by the U. S. Army Research Office -- Durham under Grant DA-ARO-D-31-124-G-317.

ACKNOWLEDGMENT

The author is deeply indebted to Professor J. R. Singer for his continued encouragement and support. Many illuminating discussions with Professors N. Bloembergen and S. E. Schwarz contributed greatly to the experimental interpretation and the theoretical approach presented in this thesis. Invaluable technical aid was received from M. Pedinoff, C. Asawa, and D. Devor of the Hughes Research Laboratories in the initial experimental phases. In particular, the author would like to thank his colleague, L. Lin, for his continuing interest and his selfless experimental assistance. Also the author is grateful to the Hughes Research Laboratories for financial support on the Hughes Doctoral Fellowship and for the loan of considerable necessary equipment.

ABSTRACT

The nonlinear interaction between light and sound, known as the stimulated Brillouin effect, is examined in this paper from a theoretical and an experimental point of view. A phenomenological theory is presented in both classical and quantum mechanical languages. The bases for the designations of "parametric acoustic amplifiers" and "phonon masers" are delineated; many similarities and a few discrepancies become evident in the two descriptions. An experimental attempt at direct observation of phonon gain is outlined. Conclusive results have not been obtained because of technical difficulties, but the methodology and problems may be of interest to the reader.

I. INTRODUCTION

This paper is a discussion of the stimulated Brillouin effect. In 1922, Brillouin[1] predicted that light could be scattered from sound waves in a transparent medium. In 1964, Chiao, Townes, and Stoicheff[2] generated a photoelastic instability by parametric conversion of laser light.

The sound, Brillouin argued, is manifest as a periodic, travelling wave of varying optical density and acts as a moving transmission grating. In this way he correctly predicted the Bragg law angular dependence and Doppler frequency shift of the diffracted light. Brillouin scattering was identified later as a Raman-type process with transitions occuring between acoustic branch vibrational states in the medium. Debye and Sears[3] are credited with first having observed the effect, ten years after Brillouin's prediction. Further definitive experiments were performed by Bär[4] in 1933 and Parthasarthy[5] in 1936. In these early experiments ultrasonic waves were transduced into a medium and the diffracted quasimonochromatic light was observed. The effect has found application in detection of ultrasonics, in determination of sound velocity[6] and, recently, in modulating, phase-locking, and stabilizing lasers.[7]

The inverse reaction, photoelastic generation of hypersonic (microwave frequency) waves by intense lights, is a current topic of interest in nonlinear optics. The technique used to observe this, stimulated Brillouin scattering, to date has been the detection of a frequency shifted, reflected light wave. Mechanisms involved in creating this large effect have been variously described as classical parametric amplification or quantum parametric or maser action. An analysis by Kroll[3] is an authoritative classical picture; Yariv[9] presents

a comparable quantum development. In this paper we present the theoretical aspects of both problems in some detail and note the comparisons and discrepancies and solve for certain new possible modes of behavior.

The normal Brillouin effect has been analysed thoroughly for sound frequencies up to the microwave region. Born and Wolf,[10] Chapter 12, present a survey of the relevant classical work. Tamm,[11] in the early days of quantum field theory, treated the quantized field Brillouin effect to explain Raman scattering from a thermal distribution of acoustic excitations. To date all relevant theories describe the interaction between light and sound phenomenologically. Typically, the dielectric constant, ϵ, is modified according to a density variation from longitudinal strain waves; the Lorentz-Lorenz law is taken as the connection between ϵ and the density with the polarizability regarded as unaffected by strain. In this paper we hold to the phenomenological position because it is tractable, but we point out its limitations when necessary.

The stimulated Brillouin effect, as presently observed, gives little useful information about the true coupling parameter or the threshold (gain $\gtrsim$ loss) behavior. It has been seen only when a significant portion (1 to 10%) of the incident light is coherently scattered. This requires not only that threshold obtains, but that there also be large net gain. Aside from the limited data made available on the magnitude of the interaction, large-scale scattering tends to destroy crystals and/or to create parasitic effects such as stimulated Raman scattering, heating, and arcing in both solids and liquids. At room temperature much of this is due to the normally large phonon losses which must be overcome. As indicated by Chiao, et al,[2] a possible way of reducing the destructive effects is to lower the temperature because these phonon losses can be eliminated effectively.

In the last section of this paper we describe an experiment conducted to demonstrate Brillouin scattering at low temperatures under controlled conditions. The program is as follows:

1) Microwave phonons are generated and detected in a liquid helium-cooled quartz rod by techniques introduced by Bömmel and

Dransfeld;[12]

2) Q-switched ruby laser light is scattered from these propagating phonons;

3) Under proper conditions, phonon gain results and is detected piezoelectrically. In principle even large gains are possible without destructive effects.

4) Spontaneous phonon oscillation also is detectable in principle.

The experimental program was not successful however, for purely technical reasons. Briefly, the laser radiation interfered with the detection apparatus resulting in destruction of detection sensitivity. More will be said about this later when we discuss the instrumentation. First we develop the theory to be used as an experimental guideline.

II. LAGRANGIAN FORMULATION OF THE INTERACTION

The Lagrangian density of the fields is a convenient starting point for both the classical and quantum mechanical treatments of phonon-photon interactions. We consider an electromagnetic vector potential, $\underset{\sim}{A}(\underset{\sim}{x}, t)$, coupled to a strain wave of displacement vector, $\underset{\sim}{R}(\underset{\sim}{x}, t)$, through a density modulated dielectric constant, ϵ. In an isotropic, transparent medium, the Lorentz-Lorenz law is likely to hold.

$$(\epsilon - 1)/(\epsilon + 2) = \alpha_p \rho , \tag{1}$$

where α_p is the polarizability and ρ is the density. The change in ϵ due to a compressional wave is given by

$$\delta\epsilon = (\epsilon_0 - 1)(\epsilon_0 + 2)\,\delta\rho/3\rho_0 = -\gamma \underset{\sim}{\nabla} \cdot \underset{\sim}{R} , \tag{2}$$

where ϵ_0 and ρ_0 are the unstrained dielectric constant and density, respectively; $\underset{\sim}{\nabla} \cdot \underset{\sim}{R}$ is the longitudinal strain, and $\gamma = (\epsilon_0 - 1)(\epsilon_0 + 2)/3$.

The Lagrangian field density is now written by suitably modifying the well-known free field Lagrangians.[13,14]

$$\mathcal{L} = (1/8\pi c^2)(\epsilon_0 - \gamma \nabla \cdot \underset{\sim}{R})\dot{A}^2 - (1/8\pi)(\nabla \times \underset{\sim}{A})^2$$

$$+ \frac{\rho_0}{2}\dot{R}^2 - \frac{1}{2}\sum_{\mu\nu}\left[\alpha \frac{\partial R_\mu}{\partial x_\mu}\frac{\partial R_\nu}{\partial x_\nu} + \beta \frac{\partial R_\mu}{\partial x_\nu}\frac{\partial R_\mu}{\partial x_\nu}\right]. \qquad (3)$$

Here α and β are elastic constants of the medium, μ and ν are coordinate indices. We recognize the electric and magnetic fields

$$\underset{\sim}{E} = -\dot{\underset{\sim}{A}}/c, \quad \underset{\sim}{H} = \nabla \times \underset{\sim}{A}, \qquad (4)$$

and the usual mechanical kinetic and potential energies in the elastic continuum limit. Although we have chosen γ to be scalar, in general the coupling is a fourth rank tensor relation, $\mathcal{L}_{int} = -(1/8\pi c^2)\gamma_{\lambda\mu\nu\sigma}\dot{A}_\lambda \dot{A}_\mu \cdot (\partial R_\nu/\partial x_\sigma)$. Kroll[8] analyzes these full tensorial properties; but since most of the physics is contained in a scalar coupling, we specialize early to minimize the mathematics. The tensor properties arise from a generalized Lorentz-Lorenz law for anisotropic media and from an involved (but usually small) dependence of the atomic polarizability on the strain. For example, the latter could couple shear waves to light, and the former could mix ordinary and extraordinary light waves in an acoustically excited crystal. However, insofar as we are relying on a phenomenological description of the interaction, and since experiments are usually keyed to test the single component γ which we are considering, there is sufficient justification for simplifying at this point.

The classical equations of motion are obtained from the Lagrangian density by application of the principle of least action which yields Hamilton's equations,

$$\frac{\partial \mathcal{L}}{\partial Q} - \frac{\partial}{\partial t}\frac{\partial \mathcal{L}}{\partial \dot{Q}} - \sum_\mu \frac{\partial}{\partial x_\mu}\frac{\partial \mathcal{L}}{\partial(\partial Q/\partial x_\mu)} = 0 \qquad (5)$$

Here Q represents a general field amplitude, a component of $\underset{\sim}{A}$ or $\underset{\sim}{R}$. When the vector potential is taken, Maxwell's equation follows:

$$\partial(\epsilon \underset{\sim}{E})/\partial t = c \underset{\sim}{\nabla} \times \underset{\sim}{H} ; \tag{6}$$

when the longitudinal vector displacement is used, the stress-strain equation ensues

$$\rho_0 \ddot{\underset{\sim}{R}} - c_{11} \nabla^2 \underset{\sim}{R} - (\gamma/8\pi) \underset{\sim}{\nabla} (E^2) = 0 \tag{7}$$

where $c_{11} = \alpha + \beta$. Now with $c_s^2 = c_{11}/\rho_0$ and $c_\ell^2 = c^2/\epsilon_0$ defining the sound and light velocities, we obtain the coupled classical wave equations from Equations 4, 6, and 7.

$$\nabla^2 \underset{\sim}{R} - c_s^{-2}(\ddot{\underset{\sim}{R}} + \dot{\underset{\sim}{R}}/\tau_s) = -(\gamma/8\pi c_{11}) \underset{\sim}{\nabla} (E^2) \tag{8}$$

$$\underset{\sim}{\nabla} \times \underset{\sim}{\nabla} \times \underset{\sim}{E} + c_\ell^{-2}(\ddot{\underset{\sim}{E}} + \dot{\underset{\sim}{E}}/\tau_\ell) = (\gamma/c^2)\partial^2(\underset{\sim}{E} \underset{\sim}{\nabla} \cdot \underset{\sim}{R})/\partial t^2 \tag{9}$$

We have introduced phenomenological relaxation times, τ, to account for unavoidable losses in the free fields. From these equations we initiate a study of the classical parametric interactions; however, first we develop the formalism with a view towards quantizing the fields.

In order to obtain the Hamiltonian density, $\mathcal{H}$, from the Lagrangian, we define momentum densities conjugate to the field amplitudes

$$\pi_{A_\mu} = \partial\mathcal{L}/\partial\dot{A}_\mu = (4\pi c^2)^{-1}(\epsilon_0 - \gamma \underset{\sim}{\nabla} \cdot \underset{\sim}{R})\dot{A}_\mu \tag{10}$$

$$\pi_{R_\mu} = \partial\mathcal{L}/\partial\dot{R}_\mu = \rho_0 \dot{R}_\mu \tag{11}$$

Thus the Hamiltonian density, defined as $\mathcal{H} = \sum_\mu \left[\pi_{A_\mu} \dot{A}_\mu + \pi_{R_\mu} \dot{R}_\mu\right] - \mathcal{L}$ is given by

$$\mathcal{H} = 2\pi c_\ell^2 \left(1 + \frac{\gamma}{\epsilon_0} \underset{\sim}{\nabla} \cdot \underset{\sim}{R}\right) \pi_A^2 + \frac{1}{8\pi} (\underset{\sim}{\nabla} \cdot \underset{\sim}{A})^2$$

$$+ \frac{1}{2\rho_0} \pi_R^2 + \frac{1}{2} \sum_{\mu\nu} \left[\alpha \frac{\partial R_\mu}{\partial x_\mu} \frac{\partial R_\nu}{\partial x_\nu} + \beta \frac{\partial R_\mu}{\partial x_\nu} \frac{\partial R_\mu}{\partial x_\nu}\right]. \tag{12}$$

We have used the fact that the strain $\nabla \cdot \underset{\sim}{R} \ll \epsilon_0/\gamma$ for all cases of practical interest. Field quantization is accomplished by asserting the commutation rules

$$[A_\mu(\underset{\sim}{x}, t) , \quad \pi_{A_\nu}(\underset{\sim}{x}', t)] = i\hbar\delta_{\mu\nu}\delta(\underset{\sim}{x} - \underset{\sim}{x}') \tag{13a}$$

$$[R_\mu(\underset{\sim}{x}, t) , \quad \pi_{R_\nu}(\underset{\sim}{x}', t)] = i\hbar\delta_{\mu\nu}\delta(\underset{\sim}{x} - \underset{\sim}{x}') \tag{13b}$$

with all other commutators zero.

The classical wave equations, 8 and 9, may be derived from the Hamiltonian density by an alternative statement of Hamilton's principle

$$\pi_Q = -\frac{\partial}{\partial Q} + \sum_\mu \frac{\partial}{\partial x_\mu} \frac{\partial}{\partial(\partial Q/\partial x_\mu)} . \tag{14}$$

This equation has its quantum mechanical analogue in the Heisenberg equations of motion for the time-dependent normal mode operators. We are now able to attack specific problems by either quantum or classical techniques and to examine the similarities and discrepancies.

III. QUANTUM THEORY OF PHONON-PHOTON INTERACTIONS

A quantized theory of the parametric interactions of light and hypersonics is given by Yariv.[9] He considers coupling of single mode phonons (signal) to single mode photons (idler) by a strong, imperturbable electromagnetic field (parametric pump) in both lossless and lossy cases. We present a similar format but go beyond the Yariv treatment in three ways: 1) the parametric case is examined for full-time development including threshold and overall gain characteristics; 2) the nonparametric, three coupled mode, lossless case is solved exactly to demonstrate saturation and large pump-to-idler conversion effects; and 3) the proper place of perturbation theory is discussed.

It is seen from the Hamiltonian density (12), that shear waves do not couple to the light field and propagate undisturbed in the medium;

we do not include them further in this treatment. The electromagnetic field will be taken polarized normal to the incident plane defined by the directions of propogation of the light and longitudinal sound waves. We therefore reduce all fields to scalars in order to eliminate the necessity of attending to polarization indices; no important features are lost.

For light frequency EM waves and microwave frequency sound waves it is propitious to expand the fields in a series of plane waves normalized in a volume, V. These are eigenmodes of the free wave equations.

$$A(\underset{\sim}{x},t) = (4\pi c_\ell^2/V)^{1/2} \sum_{\underset{\sim}{k}} (\hbar/2\omega_k)^{1/2}(a_{\underset{\sim}{k}} + a^\dagger_{-\underset{\sim}{k}})e^{i\underset{\sim}{k}\cdot\underset{\sim}{x}} . \qquad (15a)$$

$$\pi_A(\underset{\sim}{x},t) = (1/4\pi c_\ell^2 V)^{1/2} \sum_{\underset{\sim}{k}} (\hbar\omega_k/2)^{1/2}\, i(a^\dagger_{\underset{\sim}{k}} - a_{-\underset{\sim}{k}})e^{-i\underset{\sim}{k}\cdot\underset{\sim}{x}} \qquad (15b)$$

$$R(\underset{\sim}{x},t) = (1/\rho_0 V)^{1/2} \sum_{\underset{\sim}{\kappa}} (\hbar/2\omega_\kappa)^{1/2}(b_{\underset{\sim}{\kappa}} + b^\dagger_{-\underset{\sim}{\kappa}})\, e^{i\underset{\sim}{\kappa}\cdot\underset{\sim}{x}} \qquad (15c)$$

$$\pi_R(\underset{\sim}{x},t) = (\rho_0/V)^{1/2} \sum_{\underset{\sim}{\kappa}} (\hbar\omega_\kappa/2)^{1/2}\, i(b^\dagger_{\underset{\sim}{\kappa}} - b_{-\underset{\sim}{\kappa}})\, e^{-i\underset{\sim}{\kappa}\cdot\underset{\sim}{x}} \qquad (15d)$$

Here the a and b expansion coefficients will be interpreted as Heisenberg operators that create or annihilate photons and phonons, respectively. The mode designations, $\underset{\sim}{k}$ and $\underset{\sim}{\kappa}$, are not essentially different but will be kept distinct to label photons and phonons. In both cases they are discrete indices ($k_x, \kappa_x = 2\pi \times \text{integer}/\ell_x$) when we assume periodic boundary conditions on the volume V. Also we take $\omega_k = kc_\ell$ and $\omega_\kappa = \kappa c_s$. The inverse transforms give

$$a_{\underset{\sim}{k}}, a^\dagger_{\underset{\sim}{k}} = V^{-1/2} \int_V d^3x e^{-i\underset{\sim}{k}\cdot\underset{\sim}{x}} [(\omega_k/8\pi c_\ell^2\hbar)^{1/2} A(\underset{\sim}{x},t)$$

$$\pm\, i(2\pi c_\ell^2/\hbar\omega_k)^{1/2} \pi_A(\underset{\sim}{x},t)] \qquad (16a)$$

$$b_{\underset{\sim}{\kappa}}, b^{\dagger}_{\underset{\sim}{\kappa}} = V^{-1/2} \int_V d^3x e^{-i\underset{\sim}{\kappa}\cdot\underset{\sim}{x}} [(\omega_\kappa \rho_0/2\hbar)^{1/2} R(\underset{\sim}{x}, t)$$

$$\pm i(1/2\hbar\omega_\kappa \rho_0)^{1/2} \pi_R(\underset{\sim}{x}, t)] \tag{16b}$$

where we have used $V^{-1} \int_V d^3x e^{i\underset{\sim}{k}\cdot\underset{\sim}{x}} = \Delta(\underset{\sim}{k})$, the Kronecker delta symbol whose value is one when $\underset{\sim}{k} = 0$, and zero otherwise.

The total Hamiltonian is formed by integrating over the volume,

$$H = \int_V d^3x = \sum_{\underset{\sim}{k}} \frac{1}{2} \hbar\omega_k (a^{\dagger}_{\underset{\sim}{k}} a_{\underset{\sim}{k}} + a^{\dagger}_{\underset{\sim}{k}}) + \sum_{\underset{\sim}{\kappa}} \frac{1}{2} \hbar\omega_\kappa (b^{\dagger}_{\underset{\sim}{\kappa}} b_{\underset{\sim}{\kappa}} + b_{\underset{\sim}{\kappa}} b^{\dagger}_{\underset{\sim}{\kappa}})$$

$$- \sum_{\underset{\sim}{k}\underset{\sim}{k}'\underset{\sim}{\kappa}} i\kappa \frac{\gamma}{\epsilon_0} \frac{\hbar^3 \omega_k \omega_{k'}}{32\omega_\kappa \rho_0 V}{}^{1/2} [(a^{\dagger}_{-\underset{\sim}{k}'} - a_{\underset{\sim}{k}'})(a^{\dagger}_{-\underset{\sim}{k}} - a_{\underset{\sim}{k}})(b_{\underset{\sim}{\kappa}} + b^{\dagger}_{-\underset{\sim}{\kappa}})] \Delta(\underset{\sim}{k}' + \underset{\sim}{k} + \underset{\sim}{\kappa}) \tag{17}$$

and is obtained from Equations 12 and 15. The term $\Delta(\underset{\sim}{k}' + \underset{\sim}{k} + \underset{\sim}{\kappa})$ indicates that momentum (wave-vector) is conserved in the interaction. Similarly, integrating the commutation relations, Equation 13, we obtain the commutators of the boson field operators

$$[a_{\underset{\sim}{k}}, a^{\dagger}_{\underset{\sim}{k}'}] = \Delta(\underset{\sim}{k} - \underset{\sim}{k}') \tag{18a}$$

$$[b_\kappa, b^{\dagger}_{\kappa'}] = \Delta(\underset{\sim}{\kappa} - \underset{\sim}{\kappa}') \tag{18b}$$

with all others zero. We now have a complete analogy to the harmonic oscillator problem, so that we may introduce states with given numbers of bosons in given modes; for example, $|n_{\underset{\sim}{k}}>$ has $n_{\underset{\sim}{k}}$ photons in mode $\underset{\sim}{k}$, and the operators act according to

$$a_{\underset{\sim}{k}} |n_{\underset{\sim}{k}}> = n_{\underset{\sim}{k}}^{1/2} |n_{\underset{\sim}{k}} - 1> ; \; a^{\dagger}_{\underset{\sim}{k}} |n_{\underset{\sim}{k}}> = (n_{\underset{\sim}{k}} + 1)^{1/2} |n_{\underset{\sim}{k}} + 1>. \tag{19}$$

Similar expressions pertain for the $b_{\underset{\sim}{\kappa}}$ and $b^{\dagger}_{\underset{\sim}{\kappa}}$ operators.

We know from standard perturbation theory that only interactions which conserve energy are likely to occur. For that reason we dispense

with the terms in the Hamiltonian of the form $(a^{\dagger}_{-\underset{\sim}{k}'}a^{\dagger}_{-k} + a_{\underset{\sim}{k}'}a_{\underset{\sim}{k}})(b_{\underset{\sim}{\kappa}} + b^{\dagger}_{-\underset{\sim}{\kappa}})$, since the energy of two light quanta cannot be balanced by a momentum conserving phonon. Also neglecting the zero point energies we can reduce the Hamiltonian to

$$H = \sum_{\underset{\sim}{k}} \hbar\omega_k a^{\dagger}_{\underset{\sim}{k}} a_{\underset{\sim}{k}} + \sum_{\kappa} \hbar\omega_{\kappa} b^{\dagger}_{\underset{\sim}{\kappa}} b_{\underset{\sim}{\kappa}} + \sum_{\underset{\sim}{k}\underset{\sim}{k}'\underset{\sim}{\kappa}} 2i\, V_{kk'\kappa} a^{\dagger}_{\underset{\sim}{k}'} a_{\underset{\sim}{k}} [b_{\underset{\sim}{\kappa}} \Delta(\underset{\sim}{k} - \underset{\sim}{k}' + \underset{\sim}{\kappa}) - b^{\dagger}_{\underset{\sim}{\kappa}} \Delta(\underset{\sim}{k} - \underset{\sim}{k}' - \kappa)], \tag{20}$$

$$V_{kk'\kappa} = (\gamma/\epsilon_0)[\hbar^3 \omega_k \omega_{k'} \omega_{\kappa} / 32 c_{\parallel} V]^{1/2}. \tag{21}$$

At this point there are two general attacks on the problem which we consider. First, we look at the time development of the Heisenberg operators, a and b, and discuss their relevance to parametric mode coupling for a few modes. Second, we apply perturbation theory and obtain results for a continuum of modes in first order.

The Heisenber equation of motion for a time-dependent operator, $0(t)$, is $i\hbar \dot{0} = [0, H]$. Applying this to a and b, we have

$$i\hbar \dot{a}_{\underset{\sim}{k}} = \hbar\omega_k a_{\underset{\sim}{k}} - \sum_{\underset{\sim}{k}'\underset{\sim}{\kappa}} 2iV_{kk'\kappa} a_{\underset{\sim}{k}'} [b^{\dagger}_{\underset{\sim}{\kappa}} \Delta(\underset{\sim}{k} - \underset{\sim}{k}' + \underset{\sim}{\kappa}) - b_{\underset{\sim}{\kappa}} \Delta(\underset{\sim}{k} - \underset{\sim}{k}' - \underset{\sim}{\kappa})], \tag{22a}$$

$$i\hbar \dot{a}_{\underset{\sim}{k}'} = \hbar\omega_{k'} a_{\underset{\sim}{k}'} - \sum_{\underset{\sim}{k}\underset{\sim}{\kappa}} 2iV_{kk'\kappa} a_{\underset{\sim}{k}} [b^{\dagger}_{\underset{\sim}{\kappa}} \Delta(\underset{\sim}{k} - \underset{\sim}{k}' - \underset{\sim}{\kappa}) - b_{\underset{\sim}{\kappa}} \Delta(\underset{\sim}{k} - \underset{\sim}{k}' + \underset{\sim}{\kappa})], \tag{22b}$$

$$i\hbar \dot{b}_{\underset{\sim}{\kappa}} = \hbar\omega_{\kappa} b_{\underset{\sim}{\kappa}} - \sum_{\underset{\sim}{k}\underset{\sim}{k}'} 2iV_{kk'\kappa} a^{\dagger}_{\underset{\sim}{k}'} a_{\underset{\sim}{k}} \Delta(\underset{\sim}{k} - \underset{\sim}{k}' - \underset{\sim}{\kappa}). \tag{22c}$$

We may simplify these equations further by transforming to the interaction picture; that is, we factor out the harmonic time dependence

$$a_{\underset{\sim}{k}} \rightarrow A_{\underset{\sim}{k}} e^{-i\omega_k t}, \quad b_{\underset{\sim}{\kappa}} \rightarrow B_{\underset{\sim}{\kappa}} \rightarrow B_{\underset{\sim}{\kappa}} e^{-i\omega_{\kappa} t}. \tag{23}$$

This introduces terms of the form $\Delta(\underset{\sim}{k} - \underset{\sim}{k}' \pm \underset{\sim}{\kappa}) \exp\{\pm i(\omega_k - \omega_{k'} \pm \omega_\kappa)t\}$ in the interaction sums on the right hand side of Equation 22. Now if we limit our considerations to just three particular modes $\underset{\sim}{k}$, $\underset{\sim}{k}'$, and $\underset{\sim}{\kappa}$, we rid ourselves of the infinite coupled mode problem which cannot be solved in detail. This confinement to three modes, electromagnetic pump and idler and acoustic signal, is valid only for a synchronous interplay of the desired modes. By synchronous, we mean that both energy and momentum are conserved.

Let us assume that we have resonance for $\omega_k = \omega_{k'} + \omega_\kappa$ and correspondingly $\underset{\sim}{k} = \underset{\sim}{k}' + \underset{\sim}{\kappa}$. This represents synchronous phonon emission into mode $\underset{\sim}{\kappa}$ with photon scattering from mode $\underset{\sim}{k}$ to mode $\underset{\sim}{k}'$. The conjugate process where a mode $\underset{\sim}{k}$ photon absorbs the phonon and scatters to mode $\underset{\sim}{k}'$ is not conservative and leaves a nonsynchronous factor $\exp\{\pm 2i\omega_\kappa t\}$ in the interaction part of the equations of motion. We discard this as a rapidly varying perturbation on the secular behavior of the system, and we reduce Equation 22 to the three mode, synchronous set

$$A_{\underset{\sim}{k}} = \Omega A_{\underset{\sim}{k}'} B_{\underset{\sim}{\kappa}}, \tag{24a}$$

$$A_{\underset{\sim}{k}'} = -\Omega A_{\underset{\sim}{k}} B^{\dagger}_{\underset{\sim}{\kappa}}, \tag{24b}$$

$$B_{\underset{\sim}{\kappa}} = -\Omega A^{\dagger}_{\underset{\sim}{k}'} A_{\underset{\sim}{k}}, \tag{24c}$$

$$\Omega = 2V_{kk'\kappa}/\hbar . \tag{24d}$$

This simple set of nonlinear equations is exactly solvable but somewhat unrealistic in the face of all of the approximations needed to obtain this form. However, before giving the solution, we will study a problem in which we attempt to take into account the effect of other modes, of normal damping and nonsynchronous transitions by introducing catch-all phenomenological lifetimes. Further, we assume that the incident mode $\underset{\sim}{k}$ is highly populated and is not affected by the interaction. Thus $A_{\underset{\sim}{k}}$ can be taken as a constant parameter which linearizes the two remaining equations:

$$\dot{B}_{\underset{\sim}{\kappa}} = -B_{\underset{\sim}{\kappa}}/2\tau_s - \Omega A_{\underset{\sim}{k}} A^{\dagger}_{\underset{\sim}{k}'} \tag{25a}$$

$$\dot{A}^{\dagger}_{\underset{\sim}{k}'} = -A^{\dagger}_{\underset{\sim}{k}'}/2\tau_\ell - \Omega A^{\dagger}_{\underset{\sim}{k}} B_{\underset{\sim}{\kappa}} . \tag{25b}$$

These are the equations obtained by Yariv[9] and identified with classical parametric amplifier equations.

The technique used to solve these equations is similar to that utilized by Kroll[8] and Bloembergen[15] to solve the classical counterparts. We try a solution of the form $B_{\underset{\sim}{\kappa}}, A^{\dagger}_{\underset{\sim}{k}'} \sim e^{-\delta t}$ which may be substituted above to get

$$\begin{bmatrix} -\delta + 1/2\tau_s & \Omega A_{\underset{\sim}{k}} \\ \Omega A^{\dagger}_{\underset{\sim}{k}} & -\delta + 1/2\tau_\ell \end{bmatrix} \begin{bmatrix} B_{\underset{\sim}{\kappa}} \\ A^{\dagger}_{\underset{\sim}{k}'} \end{bmatrix} = 0. \tag{26}$$

A unique solution may be found in terms of the eigenvalues and eigenvectors of this matrix if initial conditions are specified. The eigenvalues are obtained as roots of the determinantal equation; they are

$$\delta_{\pm} = \frac{1}{2}\left(\frac{1}{2\tau_\ell} + \frac{1}{2\tau_s}\right) \pm \left\{\frac{1}{4}\left(\frac{1}{2\tau_\ell} - \frac{1}{2\tau_s}\right)^2 + \Omega^2 A^{\dagger}_{\underset{\sim}{k}} A_{\underset{\sim}{k}}\right\}^{1/2} . \tag{27}$$

The eigenvectors corresponding to these eigenvalues are given by the ratios

$$A^{\dagger}_{\underset{\sim}{k}'\pm}/B_{\underset{\sim}{\kappa}\pm} = (\delta_{\pm} - 1/2\tau_s)/\Omega A_{\underset{\sim}{k}} . \tag{28}$$

For initial conditions suppose $A^{\dagger}_{\underset{\sim}{k}'}(0) = 0$ and $B_{\underset{\sim}{\kappa}}(0) \neq 0$. This corresponds to no initial idler photons but some phonons; we desire the gain

$$B_{\underset{\sim}{\kappa}}(t)/B_{\underset{\sim}{\kappa}}(0) = [B_{\underset{\sim}{\kappa}+} e^{-\delta_+ t} + B_{\underset{\sim}{\kappa}-} e^{-\delta_- t}]/[B_{\underset{\sim}{\kappa}+} + B_{\underset{\sim}{\kappa}-}], \tag{29}$$

where $A^{\dagger}_{\underset{\sim}{k}'}(0) = 0 = A^{\dagger}_{\underset{\sim}{k}'+} + A^{\dagger}_{\underset{\sim}{k}'-}$. Algebraically manipulating Equations 27, 28, and 29, we obtain the expression for amplitude gain :

$$B_{\underset{\sim}{\kappa}}(t)/B_{\underset{\sim}{\kappa}}(0) = \exp\{-\frac{t}{2}\left(\frac{1}{2\tau_\ell} + \frac{1}{2\tau_s}\right)\}\left[\cosh \sigma t + \frac{1}{2\sigma}\left(\frac{1}{2\tau_\ell} - \frac{1}{2\tau_s}\right)\sinh \sigma t\right], \tag{30}$$

$$\sigma = \left\{\frac{1}{4}\left(\frac{1}{2\tau_\ell} - \frac{1}{2\tau_s}\right)^2 + \Omega^2 A_{\underset{\sim}{k}} A_{\underset{\sim}{k}}^\dagger\right\}^{1/2}. \tag{31}$$

This amplitude gain factor is easily interpreted classically but leads to difficulty when applied quantum mechanically. A proper quantum treatment would ask for the expectation value $\langle \bar{n}_{\underset{\sim}{\kappa}} \bar{n}_{\underset{\sim}{k}'} | B_{\underset{\sim}{\kappa}}^\dagger B_{\underset{\sim}{\kappa}} | \bar{n}_{\underset{\sim}{k}'} \bar{n}_{\underset{\sim}{\kappa}} \rangle$ as a function of time. The state $|\bar{n}_{\underset{\sim}{k}'} \bar{n}_{\underset{\sim}{\kappa}}\rangle$ should be a coherent construction of initial boson states with average populations $\bar{n}_{\underset{\sim}{k}'}$ and $\bar{n}_{\underset{\sim}{\kappa}}$ in modes $\underset{\sim}{k}'$ and $\underset{\sim}{\kappa}$. Louisell, Yariv, and Seigman[16] demonstrate that a Poisson distribution most closely approximates the classical conditions of minimum amplitude-phase uncertainty and that such an initial state yields

$$|B_{\underset{\sim}{\kappa}}(t)/B_{\underset{\sim}{\kappa}}(0)|^2 \approx \langle \bar{n}_{\underset{\sim}{\kappa}} 0 | B_{\underset{\sim}{\kappa}}^\dagger B_{\underset{\sim}{\kappa}} | 0 \bar{n}_{\underset{\sim}{\kappa}} \rangle / \bar{n}_{\underset{\sim}{\kappa}} \tag{32}$$

apart from factors $1/\bar{n}_{\underset{\sim}{\kappa}}$.

In the case where there is no incident pump $A_{\underset{\sim}{k}}^\dagger A_{\underset{\sim}{k}} = 0$ and

$$B_{\underset{\sim}{\kappa}}(t)/B_{\underset{\sim}{\kappa}}(0) = e^{-t/2\tau_s} \tag{33}$$

as seen from Equation 30; there is only the expected loss. When $\Omega^2 A_k^\dagger A_k >> \frac{1}{4}\left(\frac{1}{2\tau_\ell} - \frac{1}{2\tau_s}\right)^2$ we have the possibility of gain where

$$B_{\underset{\sim}{\kappa}}(t)/B_{\underset{\sim}{\kappa}}(0) \simeq \exp\{-\frac{t}{2}\left(\frac{1}{2\tau_\ell} + \frac{1}{2\tau_s}\right)\} \cosh \Omega (A_{\underset{\sim}{k}}^\dagger A_{\underset{\sim}{k}})^{1/2} t. \tag{34}$$

In this domain, above threshold if $\Omega(A_{\underset{\sim}{k}}^\dagger A_{\underset{\sim}{k}})^{1/2} > \frac{1}{2}\left(\frac{1}{2\tau_\ell} + \frac{1}{2\tau_s}\right)$, the exponential gain increases with the square root of the incident light

intensity. These conditions hold for Q-switched ruby laser light incident on a quartz crystal at liquid helium temperatures. At room temperatures, τ_s is so short that $\Omega^2 A_{\underset{\sim}{k}}^\dagger A_{\underset{\sim}{k}} << \frac{1}{4}(\frac{1}{2\tau_\ell} - \frac{1}{2\tau_s})^2$ but gain is still possible.

This is demonstrated by expanding the square root, σ, so that

$$B_{\underset{\sim}{k}}(t)/B_{\underset{\sim}{k}}(0) \simeq e^{-t/2\tau_s} - \left[\Omega^2 A_{\underset{\sim}{k}}^\dagger A_{\underset{\sim}{k}}/(\frac{1}{2\tau_\ell} - \frac{1}{2\tau_s})^2\right] \times \left\{\exp\left[-\frac{t}{2}(\frac{1}{\tau_\ell} + \frac{4\Omega^2 A_{\underset{\sim}{k}}^\dagger A_{\underset{\sim}{k}}}{(\tau_\ell^{-1} - \tau_s^{-1})}\right] + \exp\left[-\frac{t}{2}(\frac{1}{\tau_s} - \frac{4\Omega^2 A_{\underset{\sim}{k}}^\dagger A_{\underset{\sim}{k}}}{(\tau_\ell^{-1} - \tau_s^{-1})}\right]\right\}. \tag{35}$$

Here we have the possibility of exponential gain proportional to the incident light flux; if $\tau_\ell < \tau_s$ then the last exp in the curly bracket is responsible and if $\tau_\ell > \tau_s$ the first exp grows. If either lifetime is much larger than the other we have the threshold condition

$$\Omega^2 A_{\underset{\sim}{k}}^\dagger A_{\underset{\sim}{k}} > 1/4\,\tau_\ell \tau_s . \tag{36}$$

Chiao et al.[2] performed their original experiments in this domain. Condition (36) has also been derived by Yariv.[9]

We now return to the three-mode lossless case, Equation 24, allowing the pump amplitude to vary according to the power it gives up to the signal and idler modes. It is convenient to introduce the notation of Feynman, Vernon and Hellwarth.[17]

$$r_0 = A_{\underset{\sim}{k}}^\dagger A_{\underset{\sim}{k}} + A_{\underset{\sim}{k}'}^\dagger A_{\underset{\sim}{k}'}, \qquad r_0(0) = R_0 \tag{37a}$$

$$r_1 = A_{\underset{\sim}{k}}^\dagger A_{\underset{\sim}{k}'} + A_{\underset{\sim}{k}'}^\dagger A_{\underset{\sim}{k}}, \qquad r_1(0) = R_1 \tag{37b}$$

$$r_2 = i(A_{\underset{\sim}{k}}^\dagger A_{\underset{\sim}{k}'} - A_{\underset{\sim}{k}'}^\dagger A_{\underset{\sim}{k}}), \qquad r_2(0) = R_2 \tag{37c}$$

$$r_3 = A_{\underset{\sim}{k}}^\dagger A_{\underset{\sim}{k}} - A_{\underset{\sim}{k}'}^\dagger A_{\underset{\sim}{k}'}, \qquad r_3(0) = R_3 \tag{37d}$$

The equations of motion for the r "vector" are obtained directly from Equation 24,

$$\dot{r}_0 = 0 \tag{38a}$$

$$\dot{r}_1 = -\Omega r_3 (B^{\dagger}_{\underset{\sim}{\kappa}} + B_{\underset{\sim}{\kappa}}), \tag{38b}$$

$$\dot{r}_2 = -\Omega r_3 (B^{\dagger}_{\underset{\sim}{\kappa}} - B_{\underset{\sim}{\kappa}}), \tag{38c}$$

$$\dot{r}_3 = \Omega [B^{\dagger}_{\underset{\sim}{\kappa}} (r_1 + i r_2) + B_{\underset{\sim}{\kappa}} (r_1 - i r_2)], \tag{38d}$$

$$\dot{n}_{\underset{\sim}{\kappa}} = -\frac{1}{2} r_3, \tag{38e}$$

where $n_{\underset{\sim}{\kappa}} = B^{\dagger}_{\underset{\sim}{\kappa}} B_{\underset{\sim}{\kappa}}$ and $n_{\underset{\sim}{\kappa}}(0) = N_{\underset{\sim}{\kappa}}$. Equations (38a and e) represent conservation of energy or, equivalently, the Manley-Rowe relations where the number of phonons emitted or absorbed is equal to the number of photons scattered. Also r_0 represents the total number of photons (all of which are conserved) and r_3 represents the excess number of photons in mode $\underset{\sim}{k}$ over mode $\underset{\sim}{k}'$. We may directly compute from Equation 37

$$r_0^2 = r_1^2 + r_2^2 + r_3^2. \tag{39}$$

We now make the semiclassical approximations: 1) that the expectation value of a product is equivalent to the expectation value product and 2) that the operators are equal to mode amplitudes. In this circumstance we are free to choose the phase of the B coefficients such that

$$B^{\dagger}_{\underset{\sim}{\kappa}} = B_{\underset{\sim}{\kappa}} = \eta_{\underset{\sim}{\kappa}}. \tag{40}$$

Equations 38a-e then reduce simply to

$$r_0 = R_0, \quad r_2 = R_2, \tag{41a}$$

$$\dot{r}_1 = -2\Omega r_3 \eta_{\underset{\sim}{\kappa}}, \tag{41b}$$

$$\dot{r}_3 = 2\Omega r_1 \eta_{\underset{\sim}{\kappa}}, \tag{41c}$$

$$d(\eta^2_{\underset{\sim}{\kappa}})/dt = -\frac{1}{2}\dot{r}_3 \tag{41d}$$

with the components of r referring to expectation values. These equations are solved in Appendix A with no further approximations necessary. We introduce normalized, dimensionless variables

$$\tau = \Omega t, \tag{42a}$$

$$Z(\tau) = r_3(\tau)/(R_0^2 - R_2^2)^{1/2}, \tag{42b}$$

$$\Omega_0 = [((R_3 + 2N_{\underset{\sim}{\kappa}})Z^2(0) + R_3 Z(0))/2]^{1/2} \tag{42c}$$

$$k^2 = 2/[(1 + 2\frac{N_{\underset{\sim}{\kappa}}}{R_3})Z(0) + 1]. \tag{42d}$$

The solutions are

$$Z(\tau) = -1 + 2\,\mathrm{sn}^2[\Omega_0\tau + \phi, k], \tag{43a}$$

$$\eta^2_{\underset{\sim}{\kappa}}(\tau) = N_{\underset{\sim}{\kappa}} - \frac{1}{2}[(R_0^2 - R_2^2)^{1/2} Z(\tau) - R_3], \tag{43b}$$

$$\phi = \mathrm{sn}^{-1}[(\frac{1}{2}(Z(0) + 1))^{1/2}, k]. \tag{43c}$$

Here sn is the Jacobian elliptic sine function with modulus k. This k should not be confused with the wave vector.

The function $Z(\tau)$ represents the fractional "inversion" of the incident photon population over the scattered photons; $\eta^2_{\underset{\sim}{\kappa}}(\tau)$ signifies the number of phonons. These equations indicate that there is a periodic

exchange of photons between the two modes brought about by coupling to the phonons. This would continue indefinitely in the lossless case. It is instructive to examine these equations when $R_3 = R_0$ and $R_1 = R_2 = 0$. Such is the case when initially all the photons are in the k-mode. Here clearly $Z(0) = 1$, $\Omega_0 = (R_3 + N_{\underset{\sim}{\kappa}})^{1/2}$ and $k^2 = [1+N_{\underset{\sim}{\kappa}}/R_3]^{-1}$. The phase of the elliptic sine is $\phi = sn^{-1}(1,k) = K(k)$, which is the complete elliptic integral. Tabulated properties of elliptic functions are given by Byrd and Friedman.[18] For these initial conditions, Equation 43 reduces to

$$Z(\tau) = -1 + 2cd^2((R_3+N_{\underset{\sim}{\kappa}})^{1/2}\tau,\ k), \tag{44a}$$

$$\eta^2_{\underset{\sim}{\kappa}}(\tau) = N_{\underset{\sim}{\kappa}}\, nd^2((R_3+N_{\underset{\sim}{\kappa}})^{1/2}\tau,\ k). \tag{44b}$$

These elliptic functions may be approximated by more familiar trigonometric functions when the modulus, k, is near zero or one. Now $k \to 0$ when $N_{\underset{\sim}{\kappa}} >> R_3$; that is, the sound wave is strong and the light weak. In this limit

$$\left.\begin{aligned} Z(\tau) &= -1 + 2\cos^2 N_{\underset{\sim}{\kappa}}^{1/2}\tau \qquad (45a)\\ \eta^2_{\underset{\sim}{\kappa}}(\tau) &= N_{\underset{\sim}{\kappa}}[1 + (R_3/N_{\underset{\sim}{\kappa}})\sin^2 N_{\underset{\sim}{\kappa}}^{1/2}\tau] \qquad (45b)\end{aligned}\right\} N_{\underset{\sim}{\kappa}} >> R_3.$$

This result is analogous to the Rabi law for spin inversion; here the photon populations are inverted by an acoustic modulation. The inversion frequency is just $2N_{\underset{\sim}{\kappa}}^{1/2}\Omega$, so it depends linearly on the strain.

The opposite extreme is encountered when the incident light is intense and the initial sound excitation is low. In this region $N_{\underset{\sim}{\kappa}} << R_3$ and $k \to 1$, so for short times $(\frac{1}{4}(1-k^2)\sinh^2\sqrt{R_3}\tau + \sqrt{R_3}\tau \tanh\sqrt{R_3}\tau << 1)$

$$Z(\tau) \simeq 1 - 2(N_{\underset{\sim}{k}}/R_3)\sinh^2 R_3^{1/2}\tau \qquad (46a)$$

$$\eta^2_{\underset{\sim}{k}}(\tau) \simeq N_{\underset{\sim}{k}} \cosh^2 R_3^{1/2}\tau \qquad (46b)$$

$$N_{\underset{\sim}{k}} << R_3$$

We see from this limit that if $N_{\underset{\sim}{k}}$ is zero, the light mode k is metastable and exponential decay builds up only in the presence of phonon noise. Spontaneous phonon emission has been left out of the analysis by the semiclassical approximations used to obtain Equation 41. We can compare this result to $B_{\underset{\sim}{k}}(t)/B_{\underset{\sim}{k}}(0)$, Equation 34, for the parametric case. In the absense of losses we see that $|B_{\underset{\sim}{k}}(t)/B_{\underset{\sim}{k}}(0)|^2 = \eta^2_{\underset{\sim}{k}}(t)/N_{\underset{\sim}{k}}$ as would be expected since we assume strong pump-weak signal in both instances. The three mode analysis, however, has the advantage that infinite gain instabilities are avoided since allowance is made for pump-power depletion. A turning point is reached eventually according to Equation 44 when the acoustic wave changes phase enough to feed power back into the pump from the idler.

Another interesting case of the three-mode analysis arises when the populations of the $\underset{\sim}{k}$ and $\underset{\sim}{k}'$ photon modes are initially equal; this is usually said to be a saturation condition. However, if the choice of phases of the two light waves is such that $R_0^2 - R_2^2 \neq 0$, mode conversion is still permitted according to Equations 42 and 43. This process of enhancing phonon gain by deliberate introduction of properly phased idler is a well known classical procedure. Kroll[8] describes this as "driven acoustical excitation" for this particular interaction system.

As a final technique under the heading of a quantum analysis, we briefly discuss the relevance of perturbation theory to the semiclassical parametric theory that has preceded. We find that first order results show some phase insensitivity and that the saturation phenomenon appears to limit mode conversion. However, the perturbation theory does attempt to legitimize the role of the continuum of states so handily discarded in the semiclassical picture. We find, in fact, that there is direct correspondence between the highly damped parametric theory, Equation 35, and

first order perturbation theory. Thus it appears that the phenomenological lifetime is a passable device to account for the extraneous mode coupling.

The standard result of first order perturbation theory for large times is the transition probability per unit time[19]

$$W_{I\to F} = (2\pi/\hbar)\left|\left\langle F\left|H_{int}\right|I\right\rangle\right|^2 \rho_E , \tag{47}$$

where $|I\rangle$ is the initial state, $\langle F|$ is the final state with the same energy as $|I\rangle$, H_{int} is the interaction part of the Hamiltonian, and ρ_E is the density of states per unit energy. The interaction part of the Hamiltonian is obtained is obtained from the third term on the right of Equation 20; it is non-diagonal in boson occupation number. If the initial state contains $n_{\underset{\sim}{k}}$, $n_{\underset{\sim}{k}'}$ photons in modes $\underset{\sim}{k}$, $\underset{\sim}{k}'$ and $n_{\underset{\sim}{\kappa}}$ phonons in mode $\underset{\sim}{\kappa}$, the matrix elements of interest are

$$\left|\left\langle (n_{\underset{\sim}{k}}-1)(n_{\underset{\sim}{k}'}+1)(n_{\underset{\sim}{\kappa}}+1)\left|H_{int}\right|n_{\underset{\sim}{\kappa}}n_{\underset{\sim}{k}'}n_{\underset{\sim}{k}}\right\rangle\right|^2$$

$$= 4V^2_{kk'\kappa}(n_{\underset{\sim}{\kappa}}+1)(n_{\underset{\sim}{k}'}+1)\,n_{\underset{\sim}{k}}, \tag{48a}$$

which corresponds to phonon emission and

$$\left|\left\langle (n_{\underset{\sim}{k}}+1)(n_{\underset{\sim}{k}'}-1)(n_{\underset{\sim}{\kappa}}-1)\left|H_{int}\right|n_{\underset{\sim}{\kappa}}n_{\underset{\sim}{k}'}n_{\underset{\sim}{k}}\right\rangle\right|^2$$

$$= 4V^2_{kk'\kappa}n_{\underset{\sim}{\kappa}}\,n_{\underset{\sim}{k}'}(n_{\underset{\sim}{k}}+1), \tag{48b}$$

which corresponds to phonon absorption. We had to exchange $\underset{\sim}{k}$ and $\underset{\sim}{k}'$ indices to obtain Equation 48b in order to conserve energy and momentum; so we have taken advantage of the symmetry of $V_{kk'\kappa}$.

Assuming that the density of states factor is the same for emission and absorption processes, we have the net rate of emission proportional to

$$[(n_{\underset{\sim}{\kappa}}+1)(n_{\underset{\sim}{k'}}+1)\,n_{\underset{\sim}{k}} - n_{\underset{\sim}{\kappa}}\,n_{\underset{\sim}{k'}}(n_{\underset{\sim}{k}}+1)]$$

$$= n_{\underset{\sim}{\kappa}}(n_{\underset{\sim}{k}} - n_{\underset{\sim}{k'}}) + n_{\underset{\sim}{k}}(n_{\underset{\sim}{k'}}+1)\,. \qquad (49)$$

Stimulated phonon emission takes place if $n_{\underset{\sim}{k}} > n_{\underset{\sim}{k'}}$ as seen from the first term on the right. This is the basis for a phonon maser description of the light-sound interaction. The second term of the right side represents an "enhanced" spontaneous phonon emission. Such enhancement derives from the initial presence of idler photons, $n_{\underset{\sim}{k'}}$; this again is a driven acoustical excitation independent of the initial number of phonons. We recall that this appears as a result of the three-mode analysis if the phases are properly chosen. Phase insensibility is characteristic of first order perturbation theory as Bloembergen[15] indicates. Partially this is due to the random reaction on the initial state of the many extraneous states, $\langle F|$, fed by $|I\rangle$ through H_{int}. Also specification of exact occupation numbers in $|I\rangle$ leads to total uncertainty in phases -- a situation remediable in part by introducing coherent superpositions of states as mentioned previously.

If initially there is a strong pump, some signal, and no idler, then the transition probability per unit time is approximately $(2\pi/\hbar)\,4\,V^2_{kk'\kappa}n_{\underset{\sim}{\kappa}}n_{\underset{\sim}{k}}\rho_E$; so the exponential phonon gain is

$$\exp\{-t\,[\tau_s^{-1} - (2\pi/\hbar)\,4\,V^2_{kk'\kappa}n_{\underset{\sim}{k}}\rho_E]\}\,.$$

We have introduced again the relaxation time, τ_s, due to normal damping. This is identical in form to the highly damped parametric situation when we compare it with the last term of the right side in Equation 35. Thus we identify

$$2\pi\hbar\rho_E \rightarrow 4/(\tau_\ell^{-1} - \tau_s^{-1}) \sim 4\,\tau_\ell$$

when $\tau_\ell << \tau_s$. The density of states in a volume of finite length, ℓ_a,

in the direction of propagation but infinite in the transverse dimensions is $\ell_a / 2\pi\hbar c_\ell$. This results from counting plane wave modes in one dimension. The quantization length is seen to be related to the absorption length of light in the medium, $c_\ell \tau_\ell$, according to the above equation.

The results of perturbation theory are presented here only to establish qualitative connections with the parametric theory given earlier and with the classical analysis to follow. Aside from the feature of spontaneous initiation of the macroscopic process, the semiclassical pictures are adequate to describe situations of experimental interest.

IV. CLASSICAL THEORY OF HYPERSONICS-LIGHT INTERACTIONS

The classical coupled wave Equations 8 and 9, are examined now in the parametric approximation. That is, the strong pump field is considered a constant parameter of the system. The techniques for handling the resultant two-coupled linear equations are given in detail by Kroll[8] and Bloembergen,[15] and were mentioned in the previous section. Thus we have only a brief resume here in order to demonstrate certain similarities to the quantum theory.

We could expand the fields in a series of eigenmodes of the homogeneous wave equations; for example

$$\underset{\sim}{R}(\underset{\sim}{x}, t) = \sum_{\underset{\sim}{\kappa}} \underset{\sim}{R}_{\underset{\sim}{\kappa}}(t) \exp\left(i(\underset{\sim}{\kappa} \cdot \underset{\sim}{x} - \omega_\kappa t)\right), \quad \omega_\kappa = c_s \kappa .$$

This, in fact, is the same manner that the modes were brought into quantization. Here, if $\underset{\sim}{R}_{\underset{\sim}{\kappa}}(t)$ varies slowly with time compared to $\exp(i\omega_\kappa t)$, then we would obtain equations exactly analogous to Equations 22 and 24. However, with the partial differential wave equations, we have the opportunity to treat space and time symmetrically and to give up the multimode coupling which proved so cumbersome previously. We take as trial solutions

$$R(\underset{\sim}{x},t) = [F(\underset{\sim}{x},t)\exp(i(\underset{\sim}{\kappa}\cdot\underset{\sim}{x} - \omega_\kappa t)) + c.c.], \quad \omega_\kappa = c_s\kappa, \tag{50a}$$

$$E(\underset{\sim}{x},t) = [E_{\underset{\sim}{k}}\exp(i(\underset{\sim}{k}\cdot\underset{\sim}{x} - \omega_k t)) + G_1(\underset{\sim}{x},t)\exp(i(\underset{\sim}{k}'\cdot\underset{\sim}{x} - \omega_{k'}t)) + c.c.],$$

$$\omega_k = c_\ell k, \quad \ell_{k'} = c_\ell k'. \tag{50b}$$

$E_{\underset{\sim}{k}}$ is the constant amplitude of the pump wave and $G_1(\underset{\sim}{x},t)$ is the idler amplitude. Both F and G_1 are assumed to vary slowly in space and time compared with the harmonic exponentials. In addition we require wave-vector and energy conservation

$$\underset{\sim}{k} = \underset{\sim}{k}' + \underset{\sim}{\kappa}, \quad \omega_k = \omega_{k'} + \omega_\kappa. \tag{51}$$

We have dropped the vector designations of the fields, choosing the strain to be longitudinal and the incident and reflected light to be transversely polarized, parallel to each other and perpendicular to the acoustic wave-vector.

Inserting these trial functions into the wave Equations 8 and 9, and discarding second derivatives due to slow variations, we have the secular equations

$$F + F/2\tau_s + c_s\kappa\cdot\nabla F = -(\gamma E_{\underset{\sim}{k}} c_s/16\pi c_{\parallel})G_1^*, \tag{52a}$$

$$G_1^* + G_1^*/2\tau_\ell + c_\ell k'\cdot\nabla G_1^* = -(\gamma E^*_{\underset{\sim}{k}}\kappa\omega_{k'}^2/2c_\ell^2)F. \tag{52b}$$

To put these equations in a more symmetric form, we define

$$G_1^* = [8\pi c_\ell c_{\parallel} k'\kappa/\epsilon_0 c_s]^{1/2} G, \tag{53a}$$

$$\beta' = \gamma[\omega_\kappa\omega_{k'}/32\pi c_{\parallel}\epsilon_0]^{1/2}. \tag{53b}$$

Equations 52a and b now take the form

$$\dot{F} + F/2\tau_s + c_s \underset{\sim}{\kappa} \cdot \nabla F = -\beta' E_{\underset{\sim}{k}} G, \tag{54a}$$

$$\dot{G} + G/2\tau_\ell + c_\ell \underset{\sim}{k'} \cdot \nabla G = -\beta' E^*_{\underset{\sim}{k}} F. \tag{54b}$$

These are essentially the equations given by Kroll[8] with an added loss term for the electromagnetic field.

We note that if the field amplitudes are uniform in space, $\underset{\sim}{\nabla} F = \underset{\sim}{\nabla} G = 0$; and Equation 54 is precisely the same as Equation 25 for the two, parametrically coupled, quantum field operators. This uniform field situation persists only for small times after turning on the pump wave and so is regarded as a transient condition. After steady state has been achieved, the uniformity is grossly altered as we will see presently. In the interim, before steady state is established but well after the interaction is initiated, the solutions of Equation 54 are somewhat intractable, although Kroll[8] has obtained analytical results in several limits.

We now examine the steady-state solutions of Equation 54; $\dot{F} = \dot{G} = 0$. The problem requires specification of boundary conditions. We take a slab of thickness, ℓ, in the z-direction starting from $z = 0$; the x- and y-directions are unbounded. An acoustic wave propagates in the z-direction with an initial value $F(0)$. The pump light also is taken to propagate with a positive z-component; so by wavevector conservation, the reflected light propagates with a negative z-component. Thus $G(\ell) = 0$ since there is no incident idler wave from the right. The solution is obtained in an identical manner to Equations 25 for the transient case, except now the boundary conditions for a backward wave amplifier are given in place of initial conditions.

We attempt a solution of the form $F,\ G \sim e^{-\underset{\sim}{\xi} \cdot \underset{\sim}{x}}$. Then from Equation 54

$$\begin{bmatrix} \xi - \alpha_s & -\beta' E_{\underset{\sim}{k}}/c_s \\ -\beta' E^*_k/c_\ell k' \cdot \xi & \xi + \alpha_\ell \end{bmatrix} \begin{bmatrix} F \\ G \end{bmatrix} = 0, \tag{55}$$

where the inverse absorption lengths are given by $\alpha_s = (2c_s\tau_s)^{-1}$ and $\alpha_\ell = (2c_\ell\tau_\ell|\underset{\sim}{k}' \cdot \underset{\sim}{\xi}|)^{-1}$. Now defining

$$\beta^2 = \beta'^2/c_s c_\ell |\underset{\sim}{k}' \cdot \underset{\sim}{\xi}| , \tag{56}$$

we have the eigenvalues of the matrix

$$\xi_{\pm} = \tfrac{1}{2}(\alpha_s - \alpha_\ell) \pm \{\tfrac{1}{4}(\alpha_s + \alpha_\ell)^2 - \beta^2 |E_{\underset{\sim}{k}}|^2\}^{1/2} . \tag{57}$$

We have defined α_s, α_ℓ, and β^2 as positive real numbers and used the fact that $\underset{\sim}{k}' \cdot \underset{\sim}{\xi} < 0$ since G travels to the left. The corresponding eigenvectors are

$$G_{\pm} = [(\xi_{\pm} - \alpha_s)/(\beta' E_{\underset{\sim}{k}}/c_s)] F_{\pm} . \tag{58}$$

The boundary conditions given above require

$$G(\ell) = 0 = G_+ e^{-\xi_+ \ell} + G_- e^{-\xi_- \ell} , \tag{59}$$

so the overall amplitude gain is

$$\begin{aligned} F(\ell)/F(0) &= [F_+ e^{-\xi_+ \ell} + F_- e^{-\xi_- \ell}]/[F_+ + F_-] \\ &= [\xi_+ - \xi_-]/[(\xi_+ - \alpha_s)e^{\xi_- \ell} - (\xi_- - \alpha_s)e^{\xi_+ \ell}] \end{aligned} \tag{60}$$

after a little algebra. Denoting

$$\zeta = \{\tfrac{1}{4}(\alpha_s + \alpha_\ell)^2 - \beta^2 |E_{\underset{\sim}{k}}|^2\}^{1/2} , \tag{61}$$

we see that the gain may be written

$$F(\ell)/F(0) = \exp\left(-\frac{\ell}{2}(\alpha_s - \alpha_\ell)\right)/\left[\cosh\zeta\ell + \frac{(\alpha_s+\alpha_\ell)}{2\zeta}\sinh\zeta\ell\right]. \quad (62)$$

If the losses are low compared to the coupling term, ζ is a pure imaginary number. In fact if $\beta^2 E_{\underset{\sim}{k}}^{\ 2} >> (\alpha_s+\alpha_\ell)^2/4$,

$$F(\ell)/F(0) \cong \exp\left(-\frac{\ell}{2}(\alpha_s - \alpha_\ell)\right)\sec\left(\beta|E_{\underset{\sim}{k}}|\ell\right). \quad (63)$$

Thus we have the possibility of infinite gain if $\beta|E_{\underset{\sim}{k}}|\ell \geq \pi/2$. This instability has been noted before the Kroll;[8] it would be limited in practice by pump depletion or crystal breakage, or -- as Kroll suggests -- nonattainment of steady state. It is clear that for ζ real there can be no instability, so we need for threshold, as given previously by Chiao et al.,[2]

$$\beta^2|E_{\underset{\sim}{k}}|^2 > (\alpha_s+\alpha_\ell)^2/4. \quad (64)$$

Stable gain, according to $\alpha_s - \beta^2|E_k|^2/\alpha_s$, is still possible below the threshold (64).

The classical analysis thus repeats the quantum analysis for parametric transient solutions and also allows a convenient description of steady state effects.

V. THEORETICAL RESUME AND CALCULATIONS

In the preceding analyses we have obtained several expressions for phonon gain under different circumstances. We now compute the expected results for the corresponding experimental conditions. First we recall that energy and momentum are conserved in all situations; we are able to represent this in the following diagram:

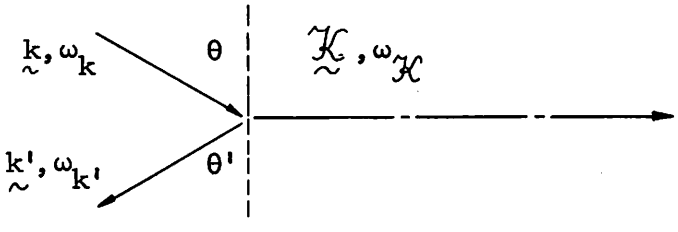

Fig. 1. Synchronous phonon emission.

The incident light has wavevector $\underset{\sim}{k}$ and frequency ω_k while the scattered light and emitted sound have respective values $\underset{\sim}{k}'$, $\omega_{k'}$ and $\underset{\sim}{\kappa}$, ω_κ. Because of the discrepancy in velocities of sound and light, the sound frequency for comparable wavelengths. For that reason $k \simeq k'$ and $\theta \simeq \theta'$. Thus matching momentum in the κ direction we obtain the Bragg law

$$\kappa \simeq 2k \sin\theta . \tag{65}$$

We see that directly backscattered light, $\theta = \pi/2$, interacts with phonons of the highest frequency. Also in a beam of finite width, the longest interaction path obtains for collinearly propagating phonons and photons. For these reasons we specialize to a one-dimensional geometry in an experimental situation.

A dispersion diagram for one-dimensional propagation yields much information about synchronous and nonsynchronous interactions; we give a simplified, exaggerated illustration below:

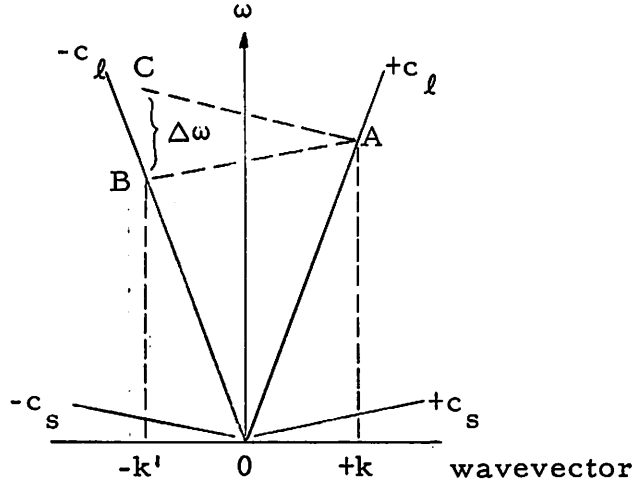

Fig. 2. Energy-momentum relations in a dispersionless medium.

In a dispersionless medium, the light and sound loci are represented by lines of slope $\pm c_\ell$ and $\pm c_s$ depending on the propagation direction. Extension to media with dispersion is trivial and need not be considered here. Incident light in mode $\underset{\sim}{k}$ is denoted by point A, reflected light by B; and the line AB with slope $+c_s$ represents the emitted phonon. The closed triangle OAB represents synchronism. Phonon absorption from $-\underset{\sim}{\kappa}$ however, is nonsynchronous as demonstrated by the line AC. The frequency mismatch, $\Delta\omega$, is seen from the diagram to be $2\omega_\kappa$; this is always true, even in three dimensions. The probability for such a nonsynchronous absorption to occur, compared to the synchronous emission is roughly $\sin^2 \Delta\omega\tau_{tr}/(\Delta\omega\tau_{tr})^2$ where τ_{tr} is the transit time of light in the medium. This is a standard result from perturbation theory or other coherence theories where $\Delta\omega\tau_{tr}$ takes the form $\Delta k\ell$. τ_{tr} is generally the same order of magnitude in most experiments, but ω_κ can vary widely. In lower frequency ultrasonics many higher order nonsynchronous diffraction phenomena occur, whereas in the microwave region it is possible to rule out such transitions.

The experimental situation envisioned is that of ruby laser light incident on a quartz crystal. Both light and sound propagate along the crystallographic x-axis. Pertinent physical parameters of the system are

$$\lambda_{vacuum} = 6943\,\text{A (plane polarized normal to c-axis of crystal)} \tag{66a}$$

$$c_s = 5.75 \times 10^5\ \text{cm/sec (experimental value} \pm 1\%) \tag{66b}$$

$$\epsilon_0^{1/2} = 1.5405\ \text{(tabulated}^{20}\text{ - ordinary ray)} \tag{66c}$$

$$\rho_0 = 2.65\ \text{gm/cm}^3\ \text{(experimental value} \pm 0.1\%) \tag{66d}$$

$$c_{11} = 87.5 \quad 10^{10}\ \text{dynes/cm}^2\ (c_{11} = c_s^2 \rho_0) \tag{66e}$$

Since there is only pump light present initially and no idler, we have

$$R_3 = a^\dagger_{\underset{\sim}{k}} a_{\underset{\sim}{k}} = A^\dagger_{\underset{\sim}{k}} A_{\underset{\sim}{k}} = n_{\underset{\sim}{k}} = \epsilon_0 |E_{\underset{\sim}{k}}|^2 V/2\pi\hbar\omega_k = SV\sqrt{\epsilon_0}/c\hbar\omega_k . \quad (67)$$

Here S is the light flux, power per unit area; the 2π (instead of 8π) in the energy density arises from the definition of the complex field amplitude, Equation 50b.

The Bragg relation for backscattered light is

$$\kappa = 2k = 4\pi \epsilon_0/\lambda_{vacuum} = 2.78 \quad 10^5 \, cm^{-1}; \quad (68a)$$

so the phonon frequency is

$$\nu_\kappa = \omega_\kappa/2\pi = 25.5 \, gc/s . \quad (68b)$$

From Equations 21, 24d, 67 and 2, we compute

$$\Omega^2 R_3 = \gamma^2 Sk'\kappa/8\epsilon_0^2\rho_0 c_s = 2.26 \times 10^{16} \, sec^{-2} / \frac{megawatt}{cm^2} \quad (69)$$

This is an important parameter of the transient theory. Correspondingly, in the steady state theory

$$\beta^2 |E_{\underset{\sim}{k}}|^2 = \gamma^2 Sk'\kappa/16\epsilon_0^2\rho_0 c_s^2 c_\ell = 1.005 \, cm^{-2} / \frac{megawatt}{cm^2} . \quad (70)$$

We must introduce the losses in order to compute threshold and gain. The relaxation time of light is $\sim 10^{-8}$ sec, corresponding to an absorption or coherence length in quartz of $\sim 2 \times 10^2$ cm. The loss in the hypersonic wave is a sensitive function of temperature. At liquid helium temperatures the sound absorption length has been measured to be ~ 10 cm; at room temperatures it is estimated to be $\sim 10^{-3}$ cm. Lifetimes at these temperatures are then $\sim 2 \times 10^{-5}$ sec at 4°K and $\sim 10^{-9}$ sec at 300°K.

Inserting these losses in the steady-state threshold Equation 64, we obtain the following values for threshold incident light flux:

$$S_{th} \sim 2.5 \times 10^{5} \text{Mw/cm}^2 \text{ at } 300°\text{K} \tag{71a}$$

$$S_{th} \sim 2.5 \times 10^{-3} \text{Mw/cm}^{-2} \text{ at } 4°\text{K}. \tag{71b}$$

This threshold lowering at low temperatures is the motivation for the experimental program which we have pursued. In the case of Q-switched lasers, the pump is on for only $\sim 4 \times 10^{-8}$ sec. Therefore, steady state is undoubtedly not attained at low temperatures where the phonon lifetime is considerably longer than the interaction time. We look then to the transient threshold indicated by Equations 34 and 36. For this case we find

$$S_{th} \sim 1 \text{Mw/cm}^2 \text{ at } 300°\text{K} \tag{71c}$$

$$S_{th} \sim 10^{-4} \text{Mw/cm}^2 \text{ at } 4°\text{K}. \tag{71d}$$

The threshold appears to be lowered in the transient case but so is the overall gain. For example with 1Mw/cm^2 incident on a 4°K crystal of length ℓ for 4×10^{-8} sec, the transient acoustic gain from Equation 30 is $\sim e^{5}$. The steady state gain, however, is seen from Equation 63 to be infinite if $\ell \sim 1.6$ cm or more. Obviously, the steady state result cannot be applied appropriately to actual experimental conditions involving Q-switched lasers incident on cold crystals.

VI. EXPERIMENTAL PROGRAM

The purpose of this experiment is to directly measure acoustic gain resulting from the stimulated Brillouin effect. We introduce microwave phonons into a cooled quartz crystal and observe the propagation behavior in the absence of light. Then we shine a Q-switched ruby laser

pulse on the crystal and look for gain or loss of the phonons relative to the quiescent conditions.

Since we are concerned with directly backscattered light as mentioned in the previous section, we must propagate 25.5 gc/s phonons in the quartz crystal. This is far from a routine technical accomplishment; so we will return to a discussion of microwave phonon production after a brief introduction to the general plan of the stimulated Brillouin experiment.

A pulse-echo method is used to study the normal hypersonic attenuation of longitudinal waves in X-cut quartz. Figure 3 illustrates the experimental procedure.

In the upper trace on the far left we have a microwave leakage signal into the receiver; the ensuing pulses are echoes of the originally generated phonons after they have traversed a 2.52 cm long crystal and returned. A nonexponential decay envelope is evident; the principal reason for this is misalignment of the end faces of the quartz rod causing destructive interference of the echoes across the detection face. Gates[21] gives an extensive survey of this effect. In the lower trace we monitor the laser radiation. This allows us to control the delay time for laser firing so that we interact with either approaching or receding sound waves. Gain is possible only when the laser beam and sound are propagating in the same direction. In Figure 3 the light was not allowed to hit the crystal, so no interaction is present. Had there been gain, all echoes to the right of the laser pulse would be larger than the quiescent echoes.

We now have an overall picture of the purpose and methodology of the experiment. The details of microwave phonon generation and detection, some parameters of the laser, and the experimental results are to be discussed next.

A. MICROWAVE PHONONS

Hypersonic waves of frequency 25.5 gc/s and wavelength 2260 A are generated in an X-cut natural quartz rod. The rod is 2.52 cm long and 0.3 cm in diameter. End faces are flat to 1/20 sodium D-line wavelength and parallel to within 2 sec of arc; they are perpendicularly aligned

to the X-crystallographic axis within 0.5°. These conditions are necessary to reduce interference effects of the exptremely short wavelength phonons. Out of a lot of ten crystals prepared to these specifications, only six supported phonons for at least one round trip. The other four may have had strains, impurities, or dislocations causing distortion and scattering of the hypersonics; or the crystal may not have been aligned precisely enough.

Quartz is chosen as the transduction and Brillouin medium to eliminate bonding problems. Piezoelectric generation and detection of hypersonics is the only technique in use at present for frequencies of K-band and higher.[22,23] Magnetostrictive transduction has been applied at lower frequencies[24] although reduced efficiencies are to be expected as the frequency increases due to the lossy materials. Also, magnetostriction is not used for longitudinal strain wave generation in the microwave range.

The acoustic attenuation in quartz at microwave frequencies is a sensitive function of temperature; at cryogenic temperatures; the logarithmic absorption per cm goes as $\omega_\kappa T^4$ or faster.[23] In the best rods at 4.2°K, a loss of less than 0.1 db/cm has been measured.

Figures 4 and 5 illustrate the decay envelope for two different rods at the same temperature, 4.2°K. The polarity is reversed in Figures 4 and 5 due to different diode demodulators at the i-f output. These pictures, due to multiple trace exposure, are clearer than the single shot Figure 3.

When fifty or more echoes are visible, the velocity of sound can be measured to better than 1%. A value of 5.75×10^5 cm/sec was measured for the longitudinal X-directed wave. This agrees well with other measurements at a variety of frequencies[12,22,23] and indicates that quartz is quite dispersionless for sound up to the millimeter-wave region. However, this measurement of c_s produces the greatest source of uncertaintly for observation of the stimulated Brillouin gain as we will discuss in part C of this section.

The microwave cavity used to excite the quartz rod is shown in Fig. 6.

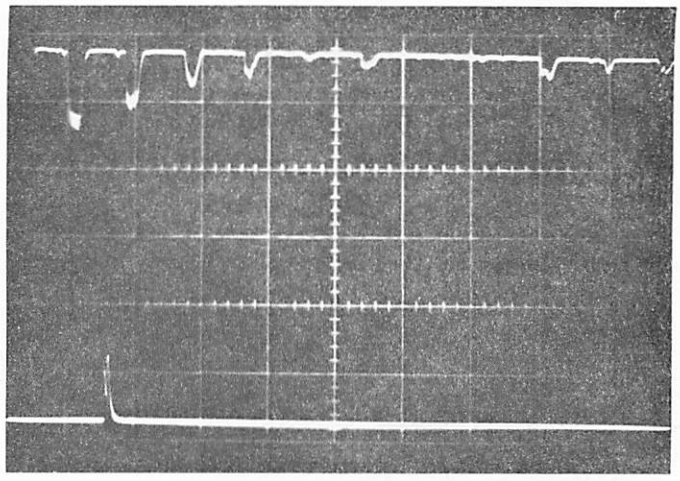

Fig. 3 Pulse-echo train and laser monitor; 10 μsec/cm.

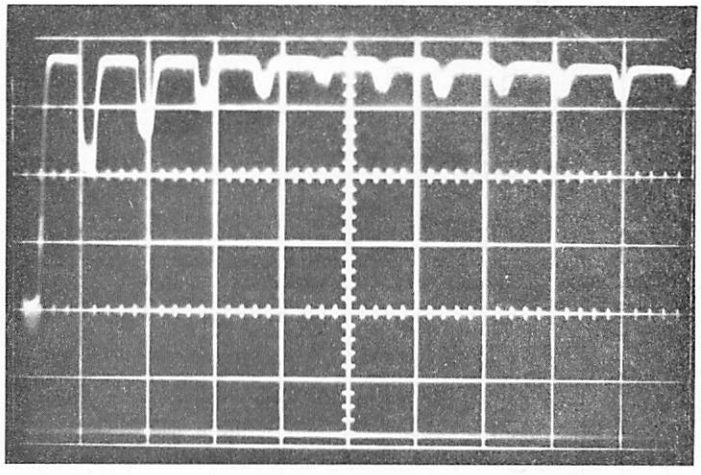

Fig. 4 Echo pattern of rod V-12; 10 μsec/cm
HP 425A square law detector.

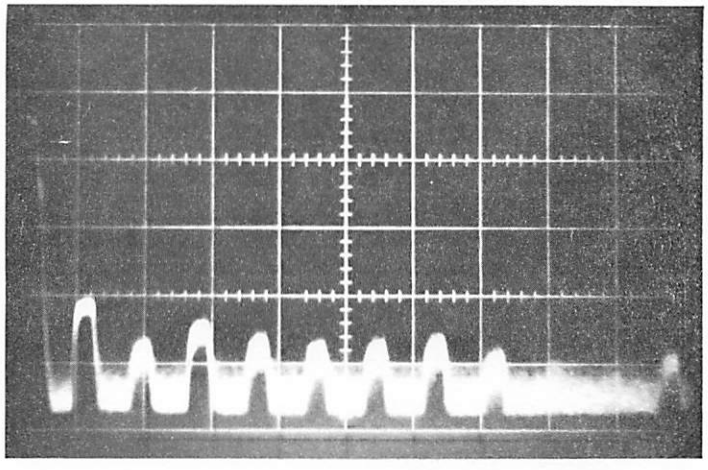

Fig. 5 Echo pattern of rod V-9; 10 μsec/cm.
Linear video detector

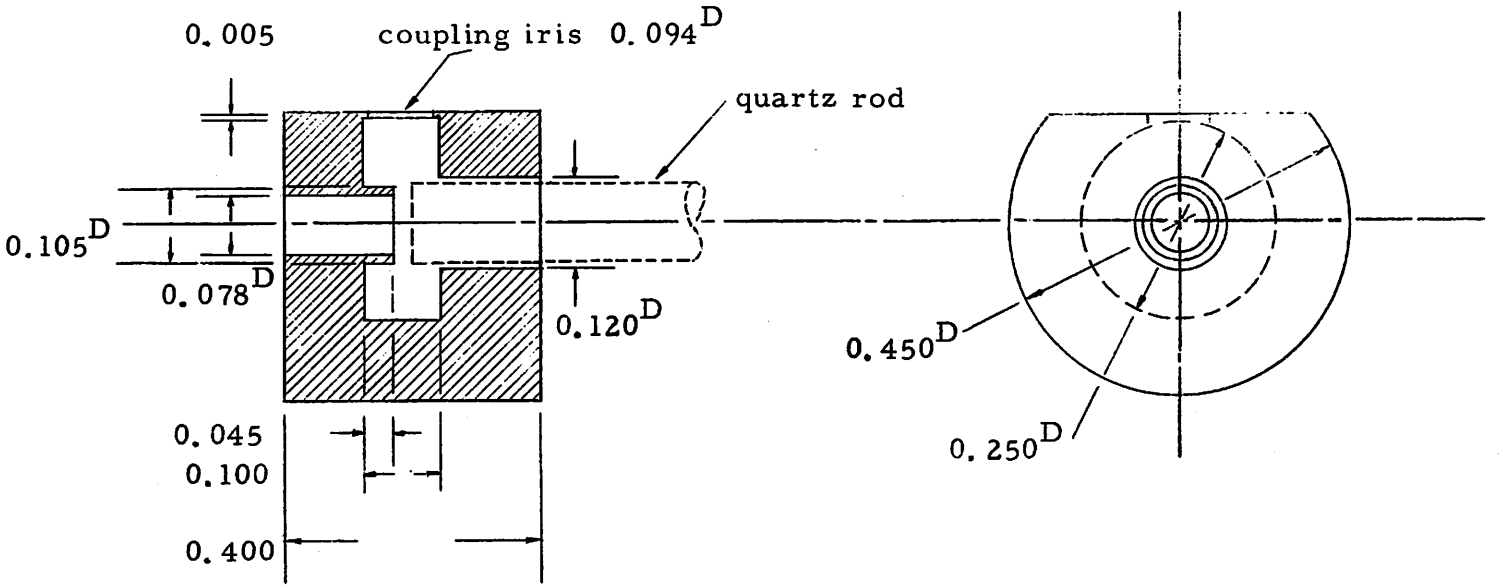

Fig. 6 K-band resonant cavity.

The cavity is a reentrant cylinder designed to enhance the electric field at the free surface of the quartz rod. It is tunable over all of K-band (18-26 gc/s) by adjusting the quartz rod position. A stub tuner is provided 1/16 in. above the coupling iris to match the cavity to the waveguide.

Cavities are machined out of copper, coin silver, or brass plated with tin or lead in order of ascending Q. Of course, the tin and lead are operated below their superconducting transition temperatures, 3.7 and 7.3°K, respectively. In this way Q's upwards of 5000 are achieved. The cavities are machined in two pieces and press fit together. Other cavities made of a single piece of copper by deposition on an aluminum mandrel show little improvement in Q and cannot be plated uniformly inside.

The overall transduction efficiency for the phonon echo experiment is defined as the microwave echo power received divided by the microwave power transmitted. It is derived in Appendix B from an equivalent circuit analysis of the electromechanical coupling. The efficiency is

$$P_{out}/P_{in} = [2M/(1+M)^2]^2 \tag{72a}$$

$$M = 2\pi d_{\parallel}^2 c_{\parallel} VQ/\epsilon_{rf} V'Q_a \tag{72b}$$

Here $d_{\parallel} = 6.9 \times 10^{-8}\ esu^{-1}$ is the piezoelectric coefficient, V is the volume of the quartz rod, Q is the cavity quality factor, $\epsilon_{rf} = 4.3$ is the dielectric constant of quartz, V' is the volume of the cavity where the electric field is stored, and Q_A is the acoustic Q of the quartz rod. $Q_A = \omega_K \tau_s$ and is generally of the order of 10^6 at helium temperatures. In a typical experiment $Q \sim 5 \times 10^3$ and $V/V' \sim 10$ so the efficiency is

$$P_{out}/P_{in} \quad -65\,db.$$

Thus the strongest echo is at least 65 db down from the transmitted pulse power which requires sensitive receiver apparatus.

A schematic diagram of the microwave transmission and detection apparatus appears in Figure 7.

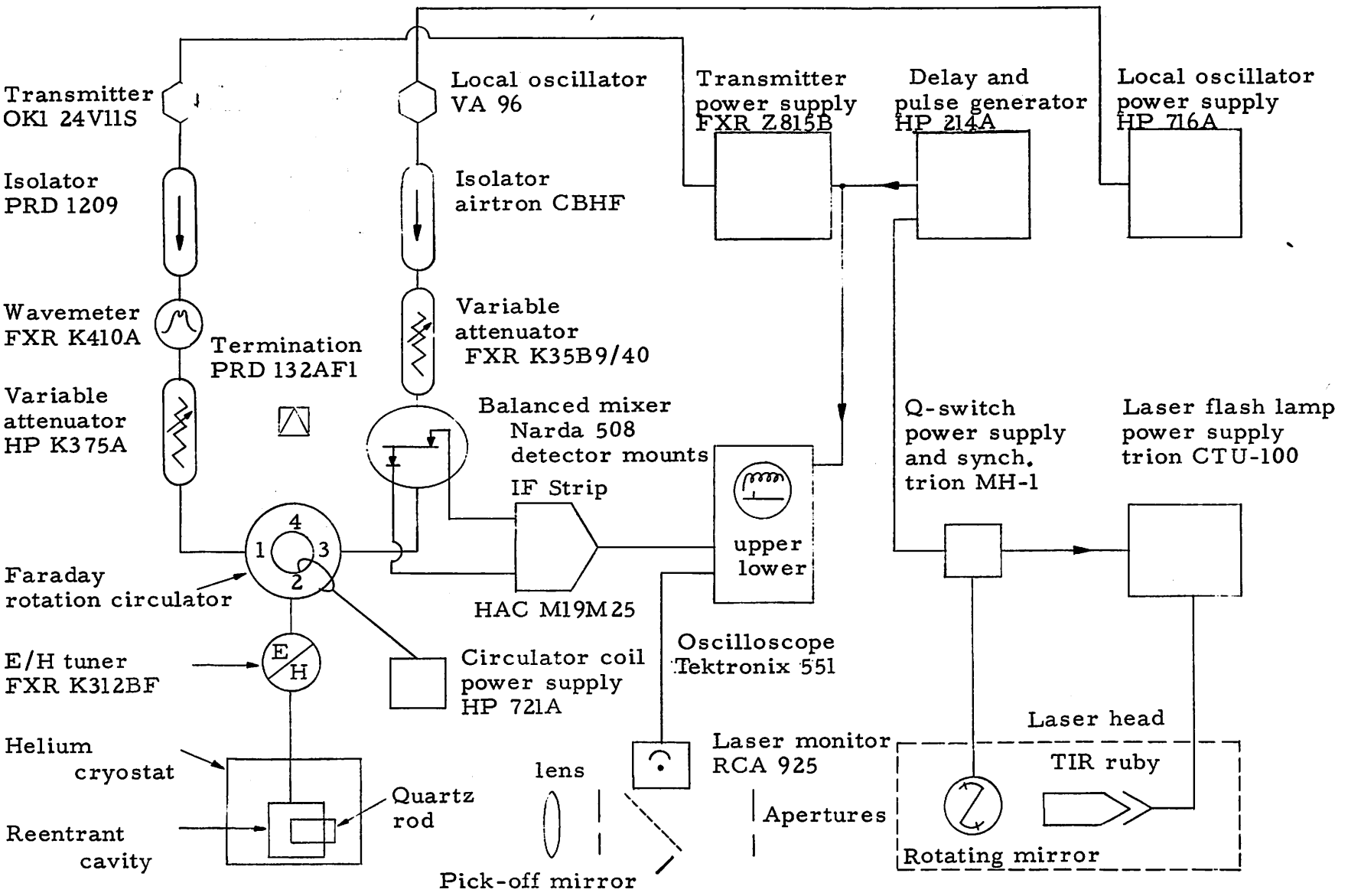

Fig. 7 Brillouin scattering system diagram.

The highest power transmitter available in the frequency range of interest is the 0KI24V11 klystron; it could deliver up to 400 mw pulsed, swept, or cw. The pulsed mode is used for phonon generation, but the swept mode is useful for tuning and matching the cavity. The cavity could be matched to better than 20 db (reflecting 1%) under most experimental conditions with the single stub tuner; however, occasionally the E/H tuner is needed as a backup in case the stub tuner jams.

A superheterodyne receiver capable of detecting signals -100 db below a watt is used to observe the phonon echoes. It consists of a balanced mixer containing forward and reverse biased 1N26 diodes, a 30 mc/s i-f strip with a 4 mc/s bandwidth, and a video detector. The local oscillator is a Varian VA-96 klystron capable of 20 mw at 25.5 gc/s. Both transmitter and local oscillator are stable within the i-f strip bandwidth with forced air cooling. Provision was made for oil bath cooling and FM-phase-locked stabilization of the VA-96 but no improvement was noted when used. However, this additional stabilization was essential when a Raytheon 2K33 klystron was incorporated as the local oscillator.

Isolators placed between the klystrons and their loads are necessary to prevent feedback instabilities under varying load conditions. A Faraday rotation circulator was built to transfer the transmitted power to the cavity and the reflected power to the receiver without the 6 db or greater insertion loss inherent in reciprocal devices such as directional couplers. A tunable dc magnetic field can be applied to the circulator to change its operating range. The 3 db insertion loss bandwidth of the circulator for fixed field is approximately 0.5 gc/s. At the peak of its frequency response, there is less than 1 db loss even for full transmitter power. The circulator is usually terminated at its fourth port with a matched load. Between the circulator and the cavity there is a section of thin-walled (0.012 in.) stainless steel wave-guide to minimize thermal conduction in the cryogenic system. This guide is silver plated to reduce microwave losses.

The insertion loss of the microwave system as a whole between the transmitter and mixer is kept to about 3 db. Therefore, with full klystron power and optimized tuning, the phonon detectivity (signal-to-noise ratio) is at most 28 db. This figure, obtained from measured losses and sensitivities and calculated transduction efficiencies, has been achieved experimentally in rare instances. Usually, thermal detuning, drift, and phonon loss result in a working detectivity of 20 db. Such a signal-to-noise ratio is not to be considered large, particularly with regard to the critically tuned cavity detection system. This, in fact, is the primary source of trouble in the Brillouin scattering experiment since the laser light can detune the cavity by a variety of methods which are discussed later.

The cavity is tuned by the mechanism shown in Fig. 8. The quartz rod is held tenuously in a collet mounted on a sliding table. Clamping the rod beyond a slip fit would result in strains that damp out the desired phonons. The sliding table is actuated by either a cam arrangement (shown) or a finely pitched screw. Similarly, the matching stub has a fine thread control.

Two helium dewars were constructed for this experiment; these are shown in Fig. 9. The glass dewar is arranged so that the microwave cavity and quartz rod are directly immersed in liquid helium; the other dewar is devised to cool by conduction. In both cases windows are provided for introduction of laser light and thin-walled stainless steel tubes connect the tuning mechanism with the experimenter. Allowance is made for pumping on the helium in both dewars to drop the temperature below the lambda point. Immersion cooling was found to be much more effective in reducing phonon loss than conduction cooling, particularly insofar as the rod is held loosely, providing a poor conduction path, and as the rod is subject to radiation through the windows. However, the noise and drift introduced by the boiling helium surface in the immersion dewar, even below the lambda point, reduces its working detectivity to that of the

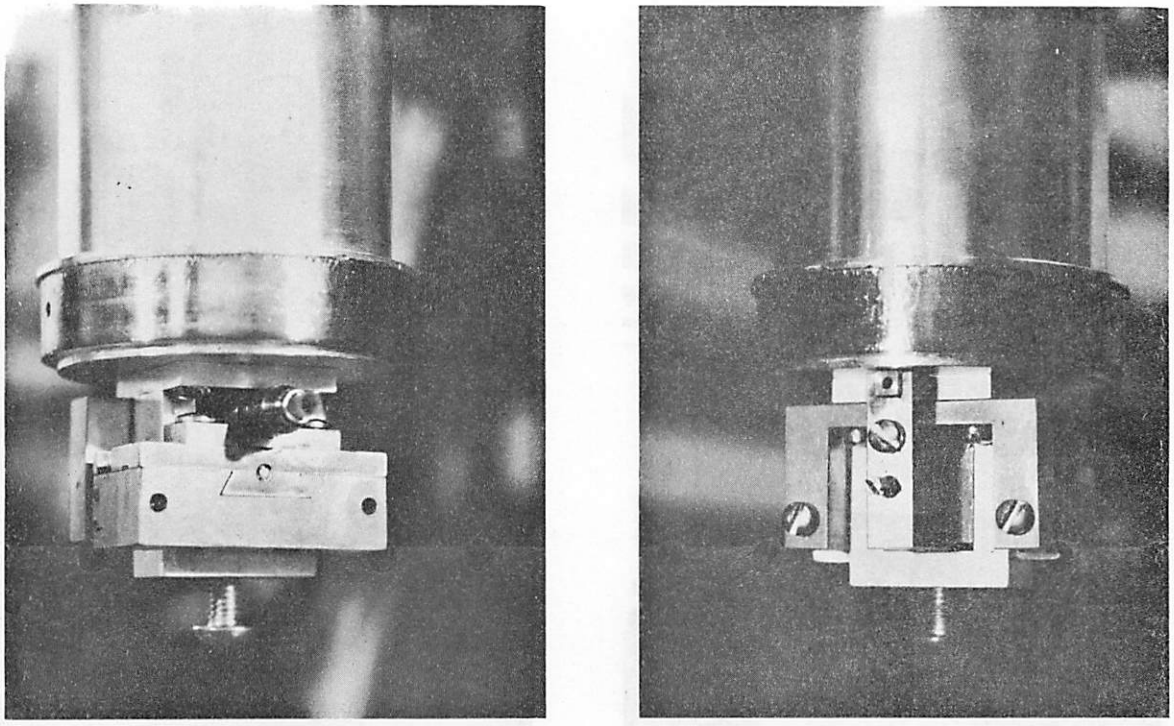

(a) Front view (b) Rear view

Fig. 8 Cavity tuning and matching arrangement.

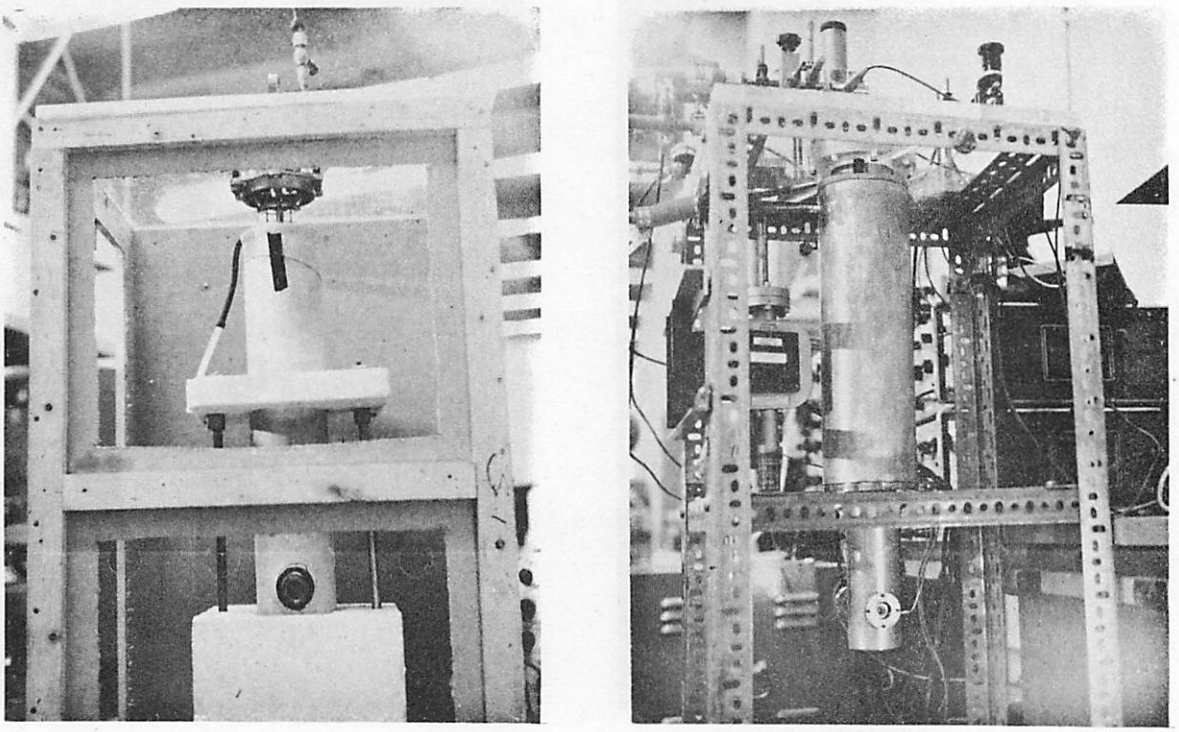

(a) Glass dewar (b) Stainless steel dewar

Fig. 9 Cryogenic systems.

stainless steel dewar. In the conduction dewar, helium is completely separated from the microwave system, in which a vacuum of 10^{-7} mm_{Hg} is maintainable by a Varian 8ℓ/s VacIon Pump.

B. LASER PARAMETERS

A Q-switched ruby laser made by Trion Instruments is used throughout this experiment. Optical cavity control is accomplished by a 60-cps rotating mirror.

Calorimetric and photometric measurement of the laser output yields the following values: at threshold, 0.01 joule in a single pulse of peak power 0.2 Mw; and at 1.35 threshold pumping energy (the maximum available), 0.10 joule in multiple pulses with largest pulse power of 0.5 Mw. The calorimeter is a one centimeter cube of copper, weighing 0.82 gm. A copper-constantan thermocouple is soldered lightly to the cube, the calorimeter is imbedded in polystyrene foam for thermal insulation, and the output (130 μvolts/joule) is read on an HP 425 A dc microvolt-ammeter. Power measurements, only roughly calibrated, are made with an RCA 925 phototube. The manufacturer's specification for the S-1 surface cathode response is accepted. A typical output of the laser is shown below; multiple pulsing is evident for 25% above threshold pumping.

Alignment of the laser beam with the acoustic wave is readily accomplished by reflecting a collimated light source off the quartz rod face through apertures defining the laser path. The Hilger-Watts autocollimator employed precisely determines the alignment to within 10 min. of arc.

The rotating mirror Q-switched generates a timing pulse approximately one millisecond before line-up and consequent laser action. This synchronization pulse is fed into an HP 214A pulse generator. Then after a delay of slightly less than the line-up time, the output of this generator is applied to the transmitter klystron reflector initiating the phonons. Synchronization of the phonon pulses with the laser output can be adjusted to within 3 μsec by this method. This is

significant jitter when compared to the phonon transit time of ~5μsec. Most of this fluctuation arises from the rotating mirror's motor speed variation.

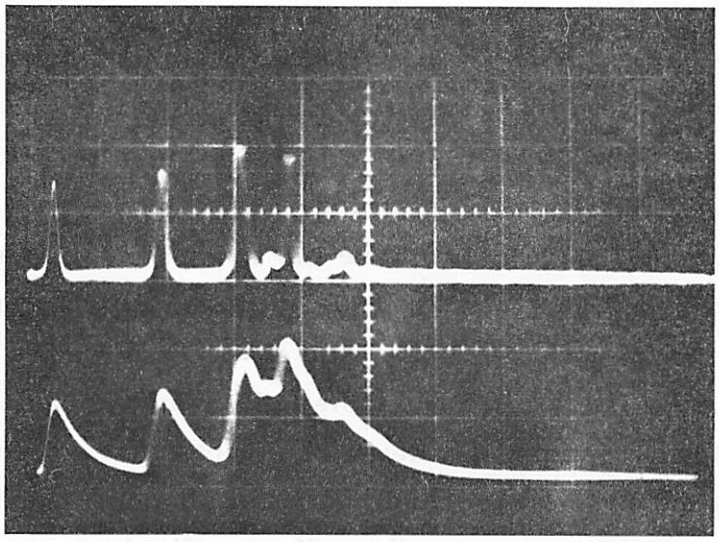

Fig. 10 Q-switched ruby laser output; 0.5 μsec/cm
Upper: Time-resulved calibrated phototube response; 0.2 Mw/cm
Lower: Laser monitor phototube.

C. EXPERIMENTAL RESULTS

Microwave phonons, in the absence of the laser, are observed with a working signal-to-noise ratio of 20 db. The laser output is known and reproducible to within 20% in energy content. Synchronization and alignment of the microwave and laser systems are achieved within workable limits. We are now in a position to discuss the problems involved when the two systems are allowed to interact. As will be seen, these problems are of sufficient magnitude to obscure all direct experimental verification of the theory.

Referring to Figure 6, we have the laser light incident from the right, passing down the quartz rod into the cavity, and focussed mildly through the hole in the back of the cavity. When the immersion cooling is used, the laser light boils the helium in the cavity, causing the quartz rod to eject and other detuning effects. This permanent detuning occurs within microseconds and all subsequent phonon echoes are lost. Figure 11 demonstrates this effect. The high noise level detected after the laser pulse is evidence of the large reflection coefficient change of the cavity when suddenly mismatched. Shot noise from the transmitter klystron beam is the source of the hash; it is usually absorbed in the cavity when matched conditions prevail.

Principally for the reason manifest in Figure 11, we see the necessity of removing the helium from the cavity by a conduction cooling scheme. Several other deteriorating effects, however, are introduced by conduction cooling. First, if the light beam does not pass cleanly through the hole in the back of the cavity, the metal inside the cavity vaporizes and deposits on the rear surface of the quartz rod. This, of course, is added loss for the microwaves and the Q is permanently reduced. No such deposition occurs with helium in the cavity, but with a pressure of 10^{-7} mm_{Hg} there is nothing to prevent it. Better alignment and sharper focussing are required to vent the light without vaporizing any metal.

As mentioned previously, because of low transmitter power, the transduction efficiency has to be maximized by raising cavity Q in order to obtain adequate detectivity. This is accomplished with

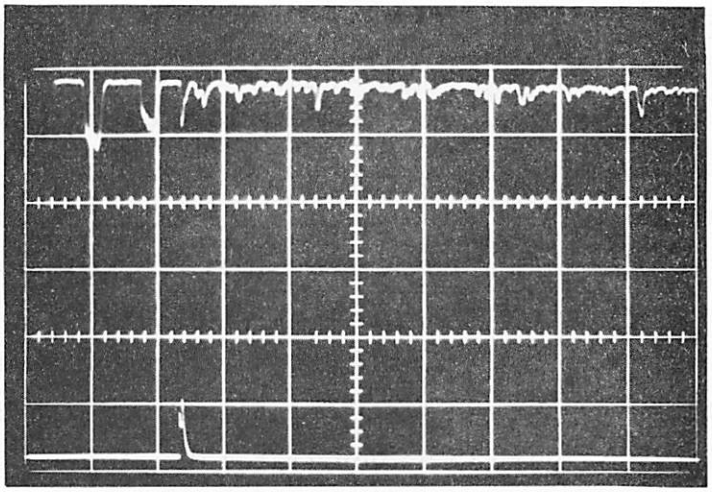

Fig. 11 Rapid, permanent detuning due to helium explosion;
10 μsec/cm
Upper: Phonon receiver output
Lower: Laser monitor.

superconductive coatings on the cavity walls. However, there is no laser power sufficient to stimulate Brillouin scattering that would not generate enough heat to destroy the superconductivity locally even when the light is perfectly vented. This results in lowered sensitivity and slight mismatch after the laser hits. However, this effect is not as drastic as the complete detuning from the helium explosion. We see this in Figure 12 where Figures 4 and 3 illustrate the same echo pattern without laser illumination (multiple and single trace, respectively). Superconductivity fully recovers in about one millisecond after the laser pulse and, as such, does not represent permanent detuning. However, the particular echo train of interest is irretrievably spoiled.

A much more temporary but severe detuning of the cavity occurs at high incident light fluxes ($\gtrsim 20\,\mathrm{Mw/cm^2}$). An example of this also appears in Figure 12 as a notch in the leading edge of the first detected echo, synchronized exactly with the laser. More dramatically, Figure 13 demonstrates the almost complete removal of the first echo without seriously affecting the second echo. Obviously, this is not a phonon-photon interaction since later echoes of the same packet show no alteration. This is completely an electrical effect traceable to an instantaneous change in cavity reflection coefficient from zero to nearly one. We see this effect explicitly in Figure 14. From this picture the threshold power dependent change is seen as the sharp spike in the upper trace. The slow reflection coefficient increase to the right of the spike is the loss of superconductivity mentioned before. This effect is quite reproducible and occurs equally with cavity pressures from atmospheric to $10^{-7}\,\mathrm{mm_{Hg}}$. Spike decay times at all pressures are faster than the instrument resolution time of $0.3\,\mu\mathrm{sec}$. (limited by receiver bandwidth).

We have described the various interferences in detection sensitivity caused by the laser. All these difficulties are produced from cavity deterioration induced by the laser. Another detrimental effect is the outright breakage of the quartz rods at light fluxes approaching $100\,\mathrm{Mw/cm^2}$. Such behavior has been noted by Giuliano.[25] Even at lower powers, some searing of the faces of the rods is evident,

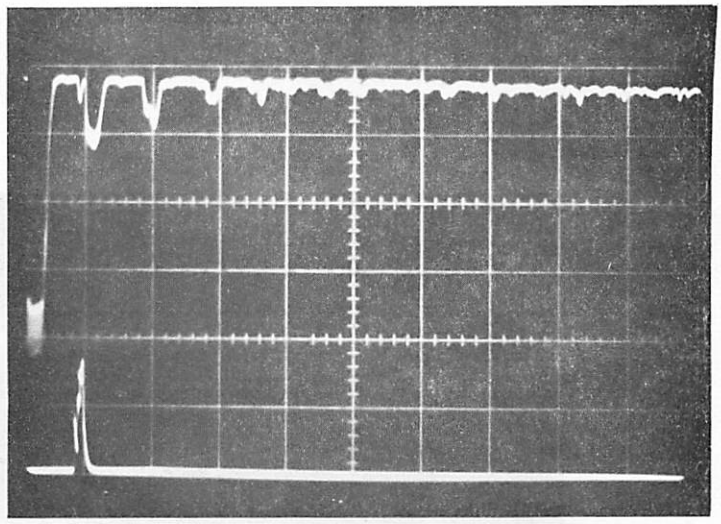

Fig. 12 Loss of superconductive sensitivity; 10 μsec/cm
Upper: Phonon receiver output
Lower: Laser monitor

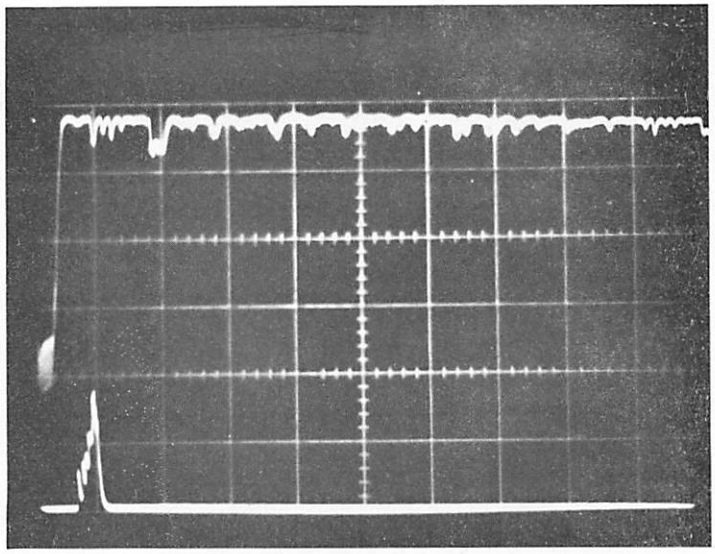

Fig. 13 Transient destruction of phonon detectivity; 10 μsec/cm
Upper: Phonon receiver output
Lower: Laser monitor, full laser power

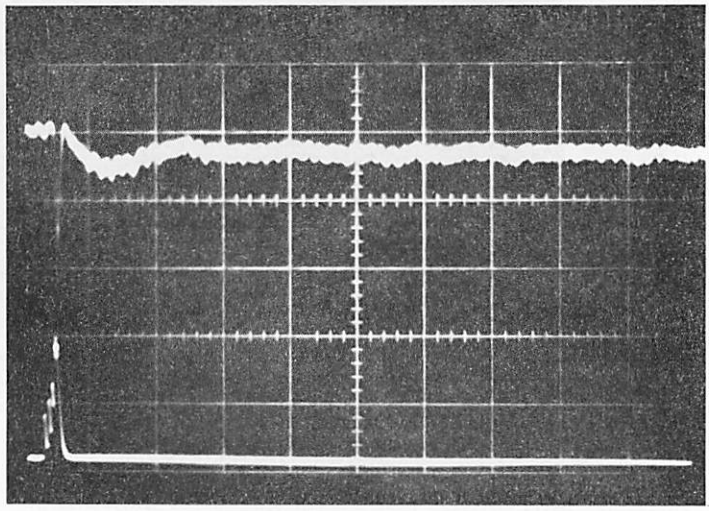

Fig. 14 Laser-induced reflection coefficient changes; 10 μsec/cm
Upper: Receiver output with CW transmitter power in
Lower: Laser monitor

and so the microwave phonons are not supported as well by the rods. Also, we must note the geometry forced upon us to minimize the electrical interferences. In Figure 6 we see that the light beam must be focused to about 1 mm in diameter to be vented from the cavity. It thus travels down the core of the rod. However, due to the hole in the reentrant post, the microwave electric fields are strongest around the perimeter of the rod. Thus the phonons are produced in an annular pattern with minimum power in the core of the rod. There is then inefficient coupling of the light and sound regions.

As a final procedural difficulty we note the tuning problem. The microwave cavity, the transmitter and the local oscillator must all be stable and tuned separately to within limits set by the receiver bandwidth of 4 mc/s. This narrow bandwidth is dictated by the sensitivity needed to receive the phonons. Because of the uncertainty in the velocity of sound, the index of refraction, and the light incidence angle, the frequency of the phonons involved in the Brillouin effect is not known to better than $\pm 1\%$. This represents a 500 mc/s band over which we must search for the interaction. Since we are probing with only a 4 mc/s window and since each laser firing causes so much deterioration, the task of finding the proper interaction frequency seems quite hopeless.

In conclusion we reiterate the, by now, clear fact that the Q-switched laser and the sensitive microwave receiver have basic incompatibilities when allowed to interact. Any future measurements attemping a direct investigation of phonon gain by the Brillouin effect should not involve these adversaries so intimately.

APPENDIX A

EXACT SOLUTION TO THREE COUPLED MODE PROBLEM

From Equations 41b, d and the initial conditions in Equations 37 and 38, we easily derive

$$\eta_{\underset{\sim}{\kappa}}^2 = N_{\underset{\sim}{\kappa}} - \frac{1}{2}(r_3 - R_3) \tag{A-1}$$

$$\dot{\eta}_\kappa = -\frac{1}{2}\Omega r_1 \tag{A-2}$$

Differentiating Equation 41c, then substituting these last relations, we have

$$r_3 = 2\Omega[\dot{r}_1 \eta_{\underset{\sim}{\kappa}} + r_1 \dot{\eta}_\kappa] = 3\Omega^2 r_3^2 - 2\Omega^2(R_3 + 2N_{\underset{\sim}{\kappa}})\, r_3 - \Omega^2(R_0^2 - R_2^2). \tag{A-3}$$

This nonlinear equation contains the excess photon density only as a dependent variable. We have used the conservation law (Equation 39) to obtain Equation A-3. We convert Equation A-3 to normalized, dimensionless form by introducing Equation 42a, b.

$$Z = 3(R_0^2 - R_2^2)^{1/2} Z^2 - 2(R_3 + 2N_{\underset{\sim}{\kappa}})\, Z - (R_0^2 - R_2^2)^{1/2}, \tag{A-4}$$

where the dot refers to differentiation by τ. This equation admits a first integral

$$\int_0^\tau Z\dot{Z}d\tau = \int_{Z(0)}^{Z(\tau)} dZ[3(R_0^2 - R_2^2)^{1/2} Z^2 - 2(R_3 + 2N_{\underset{\sim}{\kappa}})\, Z - (R_0^2 - R_2^2)^{1/2}] \tag{A-5}$$

and if we note from Equations 41c and 42b that $Z\big|_{\tau=0} = 4N_{\underset{\sim}{\kappa}}(1 - Z^2(0))$, we find easily

$$\frac{1}{2}(R_0^2 - R_2^2)^{-1/2}(Z)^2 = Z^3 - Z - (Z^2 - 1)[(R_3 + 2N_{\underset{\sim}{\kappa}})/(R_0^2 - R_2^2)^{1/2}]. \qquad (A\text{-}6)$$

This may be cast into the form of a standard elliptic integral if we factor the right hand side.

$$2(R_0^2 - R_2^2)^{1/4}\tau = \int_{Z(0)}^{Z(\tau)} dZ \quad (1-Z)(1+Z)\frac{(R_3 + 2N_{\kappa})}{(R_0^2 - R_2^2)^{1/2}} - Z^{1/2}. \qquad (A\text{-}7)$$

The result (Equation 43) follows immediately from Equation A-7 and tabulated elliptic integral No. 233.00 in Byrd and Friedman.[18]

APPENDIX B

EQUIVALENT CIRCUIT ANALYSIS OF TRANSDUCER EFFICIENCY

Two coupled resonant circuits represent the electromechanical conversion system.

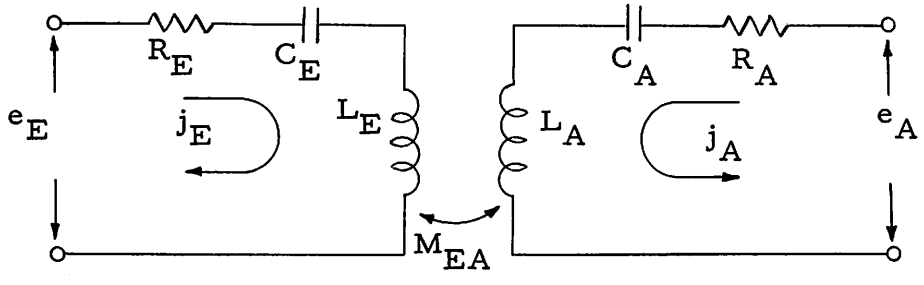

Fig. B-1 Electromechanical equivalent circuit

The circuit with subscripts E is the electrical cavity and with A the acoustic rod. The resonant frequency for both cavities is

$$\omega_\kappa^2 = (L_E C_E)^{-1} = (L_A C_A)^{-1} . \tag{B-1}$$

Cavity quality factors are

$$Q = \omega_\kappa L_A / R_A \tag{B-2}$$

$$Q_A = \omega_\kappa L_E / R_E \tag{B-3}$$

Since the stored energy in the cavity is $\epsilon_{rf} E_{rf}^2 V'/8\pi$ and the stored acoustic energy in the rod is $c_{\parallel} (\nabla \cdot R)^2 V/4$, we identify the circuit capacitances as

$$C_A = c_{\parallel} V/2 \tag{B-4}$$

$$C_E = \epsilon_{rf} V'/4\pi \tag{B-5}$$

where the voltage across the capacitors correspond to E_{rf} and $\nabla \cdot R$. The relation between this field and strain is given by the piezoelectric constant of quartz

$$\nabla \cdot R / E_{rf} = d_{\parallel} = j_A C_E / j_E C_A \tag{B-6}$$

All the above circuit elements are now defined in terms of measured quantities.

We wish to find the power delivered to the quartz rod from the cavity with no other acoustic source; that is $e_A = 0$. The power that is absorbed in the cavity from a given acoustical excitation is then computed from the first power transfer by reciprocity.

The available power into the microwave cavity is $P_{in} = |e_E|^2/2R_E$; the power absorbed in the acoustic rod is $P_A = |j_A|^2 R_A$. With no external acoustic source the circuit equations at resonance are simply

$$e_E = j_E R_E + i\omega_\kappa M_{EA} j_A \tag{B-7}$$

$$0 = i\omega_\kappa M_{EA} j_E + R_A j_A . \tag{B-8}$$

Eliminating j_E from these equations, we obtain the power transfer ratio

$$P_A/P_{in} = 2|\omega_\kappa^2 M_{EA}^2/R_E R_A|/[1+|\omega_\kappa^2 M_{EA}^2/R_E R_A|]^2 \tag{B-9}$$

An identical result obtains for P_{out}/P_A when $e_E = 0$ and $P_{out} = |j_E|^2 RE$ and the available acoustic power $P_A = |e_A|^2/2R_A$. This is just reciprocity and is equivalent to exchanging the indices E and A which changes nothing.

$$P_{out}/P_{in} = (P_A/P_{in})^2 \tag{B-10}$$

is then the overall microwave-to-acoustic-to-microwave transduction efficiency.

From Equations B-6 and B-8 we see

$$d_{\parallel} = -i\omega_\kappa M_{EA} C_E/R_A C_A . \tag{B-11}$$

Inserting this into Equation B-9 we have

$$P_{out}/P_{in} = \{2(d_{\parallel}^2 R_A C_A^2/R_E C_E^2) \quad [1+(d_{\parallel}^2 R_A C_A^2/R_E C_E^2)]^2\}^2 \tag{B-12}$$

Identifying the R's and C's in Equations B-1 through B-5, we emerge with Equations 72a and b.

REFERENCES

1. L. Brillouin, Annales de Physique, Paris, 17, 88 (1922).
2. R. Chiao, C. Townes, and B. Stoicheff, Phys. Rev. Letters, 12, 592 (1964).
3. P. Debye and F. Sears, Proc. Nat. Acad. of Sci., 18, 409 (1932).
4. R. Bar, Helvetia Physika Acta 6, 570 (1933).
5. S. Parthasarthy, Proc. Indian Acad. of Sci. A-3, 442 (1936).
6. L. Bergmann, Ultrasonics, G. Bell and Sons, Ltd., London (1938).
7. L. Foster, M. Ewy, and C. Crumly, Appl. Phys. Letters 6, 1 (1965).
8. N. Kroll, J. Appl. Phys. 36, 34 (1965).
9. A. Yariv, J. Quantum Electronics 1, 41 (1965).
10. H. Born and E. Wolf, Principles of Optics, Pergammon Press, New York (1959).
11. I. Tamm, Zeitschrift fur Physik 60, 345 (1930).
12. H. Bommel and K. Dansfield, Phys. Rev. 117, 1245 (1960).
13. H. Goldstein, Classical Mechanics Addison-Wesley Pub. Co., Cambridge (1953).
14. C. Kittel, Quantum Theory of Solids, J. Wiley and Sons, Inc., New York (1963).
15. N. Bloembergen, Nonlinear Optics, W. Benjamin, Inc., New York (1965).
16. W. Louisell, A. Yariv, and A. E. Siegman, Phys. Rev. 124, 1646 (1961)
17. R. Feynman, F. Vernon, Jr., and R. Hellwarth, J. Appl. Phys. 28, 49 (1957).
18. P. Byrd and M. Friedman, Handbook of Elliptic Integrals, Springer-Verlag, Berlin (1954).
19. E. Merzbacher, Quantum Mechanics, J. Wiley and Sons, Inc., New York (1961).
20. Handbook of Chemistry and Physics, Chem. Rubber Pub. Co., Cleveland, 43rd edition (1961).
21. E. Gates, Proc. IEEE 52, 1129 (1964).

22. E. Jacobson, Quantum Electronics I, Edited by C. Townes, Columbia Univ. Press, New York, 468 (1960).
23. J. Thaxter and P. Tannenwald, Appl. Phys. Letters. 5, 4 (1964).
24. H. Bommel and K. Dansfeld, Phys. Rev. Letters, 3, 83 (1959).
25. C. Giuliano, Appl. Phys. Letters, 5, 137 (1964).